UNIVERSITÀ
DEGLI STUDI
DI PADOVA

UNIVERSITA' DEGLI STUDI DI PADOVA

DIPARTIMENTO DI BIOLOGIA

SCUOLA DI DOTTORATO DI RICERCA IN : BIOSCIENZE E BIOTECNOLOGIE

INDIRIZZO: BIOLOGIA CELLULARE

CICLO: XXV

FRET IMAGING AND OPTOGENETICS SHED LIGHT ON NEUROCARDIAC REGULATION *IN VITRO* AND *IN VIVO*

Direttore della Scuola : Ch.mo Prof. Giuseppe Zanotti

Coordinatore d'indirizzo: Ch.mo Prof. Paolo Bernardi

Supervisore : Dott. Marco Mongillo

Dottorando : Francesca Da Broi

Index

Chapter 2

Bioinformatic and mutational analysis of channelrhodopsin-2 protein cation-conducting pathway.

Optogenetic control of sympathetic neurons activity *in vitro* and *in vivo*.

- ChR2 photostimulation modulates the activity of neuronally differentiated chromaffin cells
- ChR2 photostimulation of stellate ganglia neurons increases heart rate *in vivo*

Chapter 3

Optical modulation of cardiac activity *in vitro* and *in vivo* preliminary result

- Optical control of cardiomyocytes activity by ChR2 photostimulation *in vitro*

Optogenetic interrogation of the arrhythmia mechanism in the early phase of myocardial ischemia

Abstract

Introduction

Result

Additional discussion and conclusion

ABBREVIATIONS:

αMHC	αMHC
β-AR	beta adrenergic receptor
AM	**A**cetoxy-**M**ethyl-ester
AP	**A**ction **P**otential
Bpm	**B**eat **p**er **m**inute
cAMP	**C**yclic **A**denosine **M**onophosphate
CFP	**C**yan **F**luorescent **P**rotein
CM	**C**ardyomyocytes
ChR	**C**hannelrhodopsin
CICR	**C**alcium **I**nduced **C**alcium **R**elease
CPVT	**C**atecholaminergic **P**olymorfic **V**entricular **T**achycardia
DAD	**D**elayed **a**fter **d**epolarization
EAD	**E**arly **a**fter **D**epolarization
ECG	**E**lectro**c**ardio**g**ram
EM	**E**lectron **M**icroscopy
HS	**H**orse **S**erum
HR	**H**eart **R**ate
ID	**I**ntercalated **D**isk
NCS	**N**ew **C**alf **S**erum
NCX	**N**a^{+}/**C**a^{2+} **E**xchanger
NE	**N**orepinephrine
NGF	**N**erve **G**rowth **F**actor
PBS	**P**olyphosphate **S**aline **B**uffer
PCR	**P**olimerase **C**hain **R**eaction
PDE	**P**hopho**D**iesterase
PFA	**P**ara**F**orm**A**ldeide
PKA	**P**rotein **K**inase **A**
PNS	**P**arasympathetic **N**ervous **S**ystem

P_o	**O**pen **P**robabiliy
RyR2	**R**yanodine **R**eceptor 2
SERCA	**S**arco-**E**ndoplasmic **R**eticulum **C**a^{2+} **A**TPase
SN	**S**ympathetic **N**eurons
SNS	**S**ympathetic **N**ervous **S**ystem
SR	**S**arcoplasmatic **R**eticulum
TAE	**T**ris-**A**cetate-**E**DTA
YFP	**Y**ellow **F**luorescent **P**rotein

SUMMARY

The heart is densely innervated by sympathetic neurons (SN) that regulate cardiac function both through chronotropic and inotropic effects. During exercise and stress, SN-released norepinephrine activates cardiac beta adrenergic receptors (β-ARs) on both the conduction and contractile systems. Increased cardiac sympathetic activity leads to arrhythmias in acquired (e.g. myocardial ischemia) or inherited conditions, including **C**atecholaminergic **P**olymorphic **V**entricular **T**achycardia (CPVT), possibly *via* development of Ca^{2+} overload-dependent early- or delayed-afterdepolarizations (EAD, DAD, respectively). The DAD would serve as arrhythmogenic focus, leading to the onset of triggered activity in discrete groups of cardiac cells. Unbalanced sympathetic discharge to different regions of the heart has been identified as a potent arrhythmogenic condition [1]. In addition to the direct cardiomyocyte damage, alteration in presynaptic NE reuptake from the autonomic neuron endings, leading to catecholamine spillover in the failing myocardium [2], inducing is an arrhythmic event. These data support a model in which autonomic control of cardiac function relies on specialized sites of direct interaction between the neurons and their target cardiomyocytes (CM).
The aims of the project are:

1. To investigate whether specific cell-cell interactions have a role in the dynamics of intercellular signaling between SN and CM, aims to understand how unbalanced SN activity leads to arrhythmic condition.

2. To understand whether the unbalanced SN modulation of a limited group of cardiac cells could be involved in generating arrhythmias *in vivo,* based on an optogenetic approach

3. To study *in vivo,* non-invasively, the critical mass of myocardium necessary to generate an arrhythmogenic focus, using optogenetics.

In the first part of the project, we used an in vitro model of sympathetic neurons/cardiomyocytes (SN-CM) co-cultures to analyze the dynamics of intercellular signaling. Upon NGF treatment, SNs extend their axons and establish direct contact with CMs. NE-synthesizing terminals developed on SN at the contact site, and β1-ARs were enriched on the CM membrane in correspondence of the active release areas [3]. We performed real-time imaging using the FRET-based biosensors EPAC1-camps and AKAR3 to assess intracellular cAMP and PKA activity, respectively. Stimulation of SN was achieved using KCl or bradykinin. We observed that activation of a specific SN lead to cAMP increase in the interacting CM ($\Delta R/R_0$ = 5.6% ± 1% mean ± SEM, n = 8, AKAR3 $\Delta R/R_0$= 5.3% ± 1.5%, mean ± SEM, n=6). The cAMP response in cardiomyocytes was not due to NE released in the medium, and was absent in cells not in direct contact with the activated neuron. We showed that in cells without SN coupled the intracellular cAMP and PKA activity were not affected.

To estimate the [NE] acting on the CM β-AR at the contact site, we compared the amplitude of the FRET signal evoked by SN activation ($\Delta R/R_0$= 2.6 % ± 0.6%, mean ± SEM, n=13) to that elicited by different [NE] administered to the cell bathing solution, and we observed that the increase in the CFP/YFP ratio achieved by SN-released NE is comparable to that obtained with 3.5e-10 M NE to whole cell. Using the competitive β-antagonist propranolol we determined the effective [NE] in the 'synaptic' cleft. Competition antagonism of neuronal stimulation to CM was obtained with [Propranolol] equal to that antagonizing 100 nM of NE, indicating that such concentration is achieved in the 'synaptic cleft'. Moreover, by calculating the fraction of occupancy of the receptor at different concentration of NE we calculated that the fraction of β-ARs activated by the SN-released NE is < 1%.

2. In the second part of the project we used an optogenetic-based strategy to modulate cardiac sympathetic neurons activity non invasively *in vivo*. ChR2 is a light-gated cation channel that becomes permeable mainly to Na^+ upon light-stimulation, shown to enable control of neuronal activity both *in vitro* and in the intact brain.

We generated a mouse model expressing ChR2 in SN under the tyrosine hydroxilase (TOH) promoter. Photostimulation of the stellate ganglia neurons (SGN) was obtained in an anesthetized, open-chest model using a fiber optic to locally (1mm) deliver light

(470nm) generated from a LED. ECG recording demonstrates a rapid (100-150 ms) increase (40%±6%) in heart rate (HR) upon SGN stimulation. The extremely short activation time of the cardiac response upon ChR2 depolarization of the neurons support a model in which NE acts in a short range, consistent with direct interaction between SN and CM.

3. We used ChR2 to modulate cardiac electrophysiology. We determined in cultured neonatal cardiomyocytes that photostimulation allows triggering action potential (AP). Moreover depending on when the light pulses were given we generated normal AP, early- or delayed-aferdepolarizations (EAD or DAD). We generated a mouse model with cardiac expression of ChR2, driven by the α-MHC promoter. Optical control of cardiomyocyte membrane potential was obtained with a fiber optic, while recording the ECG in the anesthesized mouse. Stimulation was applied to different regions of the heart. Atrial illumination was used to obtain non-invasive atrial pacing resulting in tachycardia with unchanged QRS, indicating as expected that the cardiac activation wave followed the natural conduction system. Ventricular photoactivation, on the contrary, bypassing the natural conduction system gave rise to premature ventricular beats.

We provide evidence of the existence of a 'synaptic' contact between SN and CM that forms a high agonist concentration, diffusion-restricted space allowing potent activation of a small fraction of β-ARs on the CM membrane upon neuronal stimulation. SN stimulation leads to a rapid increase of the HR supporting the idea of the existence of the synaptic contact between SN and CM.

This close interaction has the potential of fast control of local CM signalling, suggesting that SNs control locally discrete groups of myocardial cells. Stimulation of a small fraction of the cardiac cells (< 200 µm-wide area) induced ectopic beats conducted to the whole heart.

RIASSUNTO

Il cuore è densamente innervato dai neuroni del sistema nervoso simpatico che regolano la funzionalità cardiaca attraverso un effetto cronotropo o inotropo positivi. Durante lo stress o l'esercizio, la noradrenalina rilasciata dai neuroni attiva i β recettori cardiaci sia sul sistema di conduzione che sul muscolo contrattile. L'aumento dell'attività del sistema nervoso simpatico cardiaco sia in condizioni normali o in presenza di patologie genetiche, come per esempio la Tachicardia Catecolaminergica Polimorfica Ventricolare, porta ad aritmie presumibilmente attraverso l'insorgere di 'DADs'. Le 'DADs' sono un *focus* di aritmia che porta a una serie di depolarizzazioni che interessano un piccolo gruppo di cellule cardiache. E' stato identificato un rilascio di catecolamine non bilanciato in diverese regioni del cuore da parte del sistema nervoso simpatico come possibile causa di aritmia. Inoltre alterazioni del *'reuptake'* di noradrenalina porta a una concentrazione anomala di NE nello scompenso cardiaco che può essere coinvolto in un evento aritmico. Questi dati supportano un modello in cui il controllo della funzionalità cardiaca da parte del sistema nervoso simpatico avviene attraverso un sito d'interazione diretta e specializzata fra neurone e cardiomiocita accoppiato.
Gli scopi del progetto sono quindi:

1. Studiare se l'interazione fra neurone e cardiomiocita ha un ruolo nella trasmissione cardiaca del segnale, per capire come un'attività non bilanciata del sistema nervoso simpatico porta a un evento aritmico.

2. Capire se l'attività non bilanciata del sistema nervoso simpatico modulando l'attività di un piccolo gruppo di cellule cardiache, possa essere coinvolto nella generazione di un'aritmia *in vivo.* Per verificare quest'ipotesi ci serviremo di un approccio innovativo basato su proteine foto attivabili.

3. Studiare *in vivo* e in maniera non invasiva la massa critica di cellule cardiache necessaria per scatenare un evento aritmico. Anche per questo tipo di studio abbiamo utilizzato una metodologia basata sull'optogenetica.

Nella prima parte del progetto, abbiamo creato un modello *in vitro* costituito da cardiomiociti neonatali e neuroni isolati dal ganglio cervicale superiore. I neuroni in seguito a trattamento con NGF sviluppano assoni che stabiliscono contatti con i cardiomiociti. Sotto terminali che sono in contatto con le cellule cardiache si osserva un maggiore accumulo di β_1 recettori [3].

Abbiamo misurato l'attivazione dei β recettori monitorando in tempo reale le variazioni di AMP ciclico e attività di PKA, attraverso l'uso di sensori geneticamente codificati e che si basano sul FRET (EPAC1-camps, che ci permette di monitorare cAMP e AKAR3 che ci permette di monitorare l'attività di PKA). I neuroni del SNS sono stati stimolati con KCl o bradichinina. Abbiamo osservato che stimolando il rilascio di noradrenalina da un neurone, l'AMP ciclico e l'attività di PKA aumentano solo nei cardiomiociti accoppiati a neurone e non nei cardiomiociti senza un contatto ($\Delta R/R_0$ = 0.056 ± 0.01 mean ± SEM, n = 8, AKAR3 $\Delta R/R_0$=5.3% ± 1.5%, mean ± SEM, n=6).

Per stimare la [NE] che agisce sui β recettori nel sito di contatto abbiamo paragonato l'ampiezza del segnale FRET generato dall'attivazione neuronale ($\Delta R/R_0$= 0.026 ± SEM) con quello generato da diverse [NE] note aggiunte alla soluzione in cui si trovano le cellule. Abbiamo osservato che l'aumento del rapporto CFP/YFP ottenuto dalla noradrenalina rilasciata dai neuroni e paragonabile a quello ottenuto con 3.5e-10 M di noradrenalina che attiva tutti i recettori.

Usando un antagonista competitivo dei β recettori (propranololo) abbiamo determinato la concentrazione di noradrenalina nel *cleft sinaptico.* La concentrazione di propranolol necessaria per abolire totalmente la risposta indotta dalla noradrenalina rilasciata dai neuroni, e pari a quella necessaria per bloccare la risposta indotta da 100 nM di noradrenalina, suggerendo che la concentrazione nel *cleft sinaptico* è dell'ordine di 100 nM. Sulla base di questi dati abbiamo quindi calcolato che la frazione recettoriale con cui interagisce la noradrenalina rilasciata dai neuroni che è inferiore all'1% del totale.

2. Nella seconda parte del progetto abbiamo usato una strategia che si basa sull'*'optogenetica'* per modulare l'attività del sistema nervoso simpatico *in vivo* e in maniera non invasiva. ChR2 è un canale la cui permeabilità è regolata dalla luce. Infatti questo canale diventa permeabile soprattutto al Na^+ in seguito a stimolazione con luce blu. Negli ultimi anni è stato largamente utilizzato per il

controllo dell'attività neuronale sia *in vitro* che *in vivo* [4, 5]. Abbiamo generato un modello murino che esprime ChR2 nei neuroni del sistema nervoso simpatico sotto il promotore tirosina idrossilasi. La foto stimolazione del ganglio stellato è stata ottenuta in un modello a 'torace aperto' di topo anestetizzato, usando una fibra ottica per indirizzare in uno specifico punto la luce generata da un LED. L'analisi dell'ECG del topo mostra un rapido (100-150 ms) aumento (40%±6%) nella frequenza di contrazione cardiaca in seguito a '*fotostimolazione*' del ganglio stellato. Questo rapido aumento nella frequenza cardiaca supporta il modello in cui la noradrenalina agisce in uno spazio piccolo e confinato in cui neurone e cardiomiocita interagisccono direttamente.

3. Abbiamo usato ChR2 anche per modulare l'elettrofisiologia cardiaca. Abbiamo determinato che la fotostimolazione di ChR2 è sufficiente a modulare il potenziale d'azione in cardiomiociti neonatali in cultura. Inoltre a seconda di quando viene dato il pulso di luce siamo in grado di generare un battito normale, una DAD o una EAD. Abbiamo quindi generato un modello di topo che esprima ChR2 nel cuore sotto il promotore α-MHC. Abbiamo controllato tramite stimolazione luminosa il potenziale d'azione di cellule cardiache utilizzando fibre ottiche alimentate da LED, durante l'acquisizione dell'ECG del topo. La stimolazione è stata eseguita in diverse regioni del cuore.
La stimolazione atriale ci ha permesso di mimare un *pacing* atriale sfociato poi una tachicardia. Abbiamo osservato che il QRS non ha variazioni rispetto al normale, indicando che l'onda di depolarizzazione segue il sistema di conduzione cardiaco. La foto attivazione ventricolare invece genera un battito prematuro dato che non segue il sistema di conduzione.

Abbiamo qui dimostrato l'esistenza di un contatto sinaptico fra i neuroni e i cardiomiociti che forma un sito a elevata concentrazione di neurotrasmettitore, uno spazio a diffusione limitata permettendo quindi l'attivazione di un ristretto gruppo di recettori β localizzati nella membrana della cellula cardiaca.
La stimolazione neuronale genera un rapido aumento nella frequenza cardiaca avvalorando l'ipotesi dell'esistenza di un contatto sinaptico fra neuroni e cardiomiociti.

Questa interazione è importante per un controllo rapido del segnale locale dei cardiomiociti, suggerendo che i neuroni controllino un gruppo ristretto di cellule cardiache. La stimolazione di una frazione di cardiomiociti è sufficiente a indurre un battito condotto in tutto il cuore.

SYMPATHETIC NERVOUS SYSTEM IN THE HEALTHY AND DISEASED HEART: EVIDENCE OF A SYNAPTIC INTERACTION.

1. The conduction system of the heart

The cardiac muscle (myocardium) is formed by terminally differentiated cells, called cardiomyocytes (CM). Working cardiac myocytes are linked one to the other by intercellular connection, forming the intercalated disk (ID)[6]. They are classified in three complexes: fascia adherens, desmosome and gap junction.

Desmosome are adhesion junction that connect the cells with the intermediate filaments in particular in area that undergoes physical stress, such as cardiomyocytes [7]. Desmosomal proteins are:

(a) Cadherins (desmogleins and desmocollins) that are essential in forming adhesive cell-cell interaction[7, 8].

(b) Plakoglobin and Plakophilins, that are cytoplasmic cadherins regulating cadherins adhesion activity[7, 8].

(c) Plakins (desmin), that binds the intermediate filaments[7, 8].

Fascia adherens are the linking between the cell membrane to the actin cytoskeleton[7, 8]. This complex is formed by:

(a) Cadherins that regulates cell-cell adhesion[7, 8].

(b) Catenin that modulate cadherine adhesive activity [7, 8].

(c) Vinculin and α-actin that link the ID to the cytoskeleton [8, 9].

Gap junctions are intercellular pores or channel formed by connexin [7, 10]. Six connexin complex interacts with another one in the adiacent cells to form hexameric hemichannel, called connexon. This complex permits the electrical coupling between the cells allowing to small molecule to pass troughout the cytoplasm of the adiacent cells[7].

Cardiac tissue is divided in two components: *working myocardium*, formed by cells that have contractile function and the *conduction system* formed by modified cardiomyocytes that propagate the electrical pulses that trigger the contraction (*pacemaker*).

The heart contracts spontaneously and rhythmically starting from atria and going to ventricles with a precise delay of activation of the two chamber to allow the atria to pump the blood into the ventricle[11].

Cardiac impulse is generated in the sinusnode and it is conducted through the atrial myocardium to the atrioventricular node. Having reached the atrio-ventricular node it is delayed to trigger the atrial contraction and to fill the ventricle before reaching the atriovenetricular axis and the Purkinje fiber to initiate the ventricle contraction to expel the blood from the venetricle chamber[11] (**FIG. 1**).

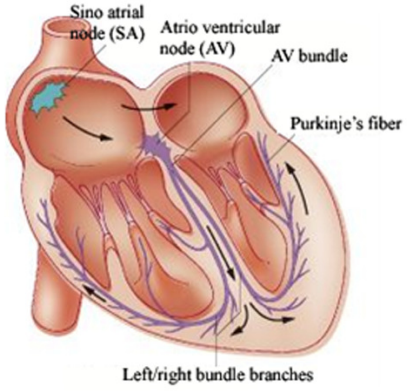

Figure 1 : Scheme of heart conduction system. Cardiac pulses is generated from the sinoatrial node (SA) and it is conducted into the atrioventricular node (AV) to trigger contraction and fill the ventricle. Through the AV axis and the Purkinje's fiber the pulse initiates ventricle contraction to expel the blood from ventricle chamber

2. Role of Ca^{2+} in normal cardiomyocytes

Proteins involved in Ca^{2+} handling constitute a critical signaling pathway in cardiac cells. At the beginning of each heartbeat, an action potentially triggers the opening of voltage-gated Ca^{2+} channels located on the plasma membrane or transverse-tubules (T-tubule), initiating Ca^{2+} flow into the cytoplasm of the cardiomyocyte. A small amount of Ca^{2+} ions are sufficient to activate a further release of Ca^{2+} from the sarcoplasmic reticulum (SR) via the ryanodine receptor (RyR2) in a process referred to as calcium-induced calcium release [12]. The increase in free [Ca^{2+}] in the cytoplasm activates the interaction between actin and myosin filaments responsible for sarcomere shortening (systole). Because a

synchronized activation of several acto-myosin cross-bridges is essential to an effective force generation, [Ca^{2+}] has to increase within a narrow time frame throughout the whole cell [13]. This is accomplished through the subcellular localization of the Ca^{2+} release sites (the RyRs), which are located in close proximity to the Ca^{2+} entry channels on the membrane, and evenly distributed with respect to Ca^{2+} sensitive sarcomeric proteins [13] [14]. For relaxation to occur at the end of the systole [Ca^{2+}] has to rapidly decrease below the threshold of activation of acto-myosin bridges. Most of the Ca^{2+} is pumped back into the SR by ATP-dependent pumps (SERCA2a) while a minor amount of Ca^{2+} is extruded from the cell by membrane-bound proteins (Plasma Membrane ATPases, Na^{+}/Ca^{2+} exchanger) [13]. The amount of force generated by the cardiomyocyte depends on the speed and amplitude of the [Ca^{2+}] rise and on its spatial distribution throughout the cellular matrix. Relaxation, by contrast, depends on how efficiently Ca^{2+} is removed from the cytoplasm.

The sympathetic nervous system (SNS) provides an important mechanism for regulating the force of cardiac contraction in response to the metabolic requirements of the peripheral organs during stress including exercise. The release of catecholamines by the SNS activates β-adrenoreceptors (β-ARs) that are coupled with G-proteins and adenylyl-cyclase, which cause elevation of the second messenger cyclic-adenosine-monophosphate (cAMP). cAMP activates protein kinase A (PKA), which phosphorylates many of the key proteins involved in Ca^{2+} handling. Phosphorylation of the Ca^{2+} channel [15] [16] and the RyR [17] leads to enhanced sensitivity to voltage and Ca^{2+}-dependent activation, respectively. The combined effect of these signaling events is an increase in the amount of Ca^{2+} available for the sarcomere during systole with a consequent increase in myocardial contractility. By contrast, PKA-dependent phosphorylation of the SERCA2a-associated protein phospholamban [18], which constitutively inhibits the activity of the pump, leads to faster Ca^{2+} removal from the cytoplasm and more efficient myocyte relaxation.

3. Cardiac sympathetic innervation

Sympathetic ganglia chain is the connection between the heart and the central nervous system [19].

Cardiac sympathetic neurons modulate cardiac activity by increasing the force and the frequency of heart contraction, mediating the response known as *'flight or fight response'*. Preganglionic sympathetic neurons are located in the central portion of the lumbar spinal cord, and project to the sympathetic ganglia chain, which runs bilaterally to the spinal cord. The superior of the sympathetic ganglia chain is the cervical ganglia, and together with the stellate ganglia it contains the bodies of the majority of the cardiac postganglionic neurons. Postaganglionic sympathetic nerves join the cardiac plexus, formed by the vagus fibers and the sympathetic neurons (SN), and run along aortic arch and reach coronary vessel to originate the coronary plexus, giving rise to the collateral branches that innervate the heart. SN innervations exhibit heterogeneous distribution inside the myocardium: the subepicardial regions displays higher SN density than the subendocardial region[20]. Sympathetic nerve fibers develop, with a mechanism regulated by NGF [21, 22], from the base of the the heart into the myocardium, and are located mainly in the subepicardium [20].

The signals are transferred from SNS to the heart through the release of catecholamines, mainly norepinephrine (NE), that interacts with the β adrenergic receptor (β-ARs) localized on the cardiomyocyte membrane. In particular during stress or exercise the activity of the sympathetic nervous system leads to a increase in the cardiovascular function through the β-ARs activation inducing an increase in the intracellular cyclic-AMP (cAMP), which in turn activates PKA, mediating phosphorylation of proteins involved in Ca2+ homeostasis, increasing the availability of Ca^{2+}, essential for sarcomere contraction, leading to an inotropic and positive chronotropic effect.

4. Beta adrenergic receptor mediated pathway

NE is released by SNS and modulates cardiac activity inducing both inotropic and positive chronotropic effects during exercise or stress. The control of cardiac activity occurs *via* activation of the β-ARs, that are G protein-coupled receptor (GPCR) localized on the membrane of the CM. NE interacts with β-ARs leading to the activation of adenylyl cyclase (AC) [23], which is the cAMP synthesizing enzyme. Cyclic-AMP activates its effectors, and in particular the cAMP-dependent protein kinase A (PKA), that phosphorylates several cytoplasm and nuclear targets. The increase in force and frequency

of heart contractions is controlled by the phosphorylation of the L-type Ca^{2+} channel [24] and the RyR2, increasing the intracellular Ca^{2+} content that are essential for sarcomere contraction during systole [25]. PKA activity is essential in the control of Ca^{2+} reuptake in the sarcoplasmic reticulum during diastole, by the phosphorylation of phospholamban (PLB) mediating the activation of SERCA proteins, that results in increased efficiency of cytosolic Ca^{2+}reuptake by the sarcoplasmic reticulum [26] (**FIG. 2**).

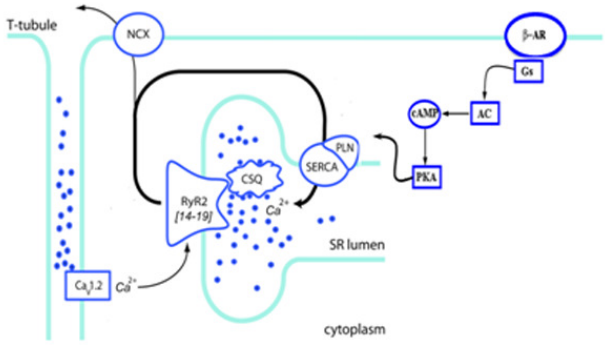

Figure 2 : Schematic representation β adrenergic pathway. NE interacts with the β-ARs induci production of cAMP. Cyclic-AMP activates PKA that phosphorylates several target proteins such as L-type Ca^{2+} channel. This allow the passage of small amount of Ca^{2+} molecules in the cytosol. Ca $^{2+}$ activates RyR2 that trigger the movements of Ca^{2+} from the Sr lumen to the cytosol increasing the cocentration of cytoplasmic Ca^{2+} allowing the contraction during systole. During diastole cytosolic Ca^{2+} is removed by NCX and SERCA.

Given the fact that NE spillover, due to SNS overactivation, occurs in patients affected by heart failure and arrhythmic events [27] and that administration of β-AR blockers is the main therapeutic strategy against arrhythmias, it becomes important to investigate whether SNS controls specifically the target cardiac cells and how the sympathetic nerve fibers exerts they control in the target CMs.

4. Beta adrenergic receptor subtype role in cardiomyocytes intracellular signaling

CMs express two major β-AR subtypes: β_1 and β_2 –ARs. Both are members of the G-protein coupled receptor (GPCR) and control the force of CM contraction through

phosphorylation of plasmalemmal and sarcomeric ion channels and contractile proteins, by increasing intracellular cAMP [28]. Stimulation of β-ARs leads to production of cAMP that activates PKA inducing phosphorylation of proteins essential in muscle contractility, mediating the catecholamine effect on cardiac performance. Although β_1-ARs and β_2-ARs are activated by the same agonist, the selective stimulation of one subtype leads to different responses in heart contractility. Indeed, alternative stimulation of the receptor elicits different physiological responses [29], and it has been suggested that activation of β_1 -AR-mediated pathway could have a role in the pathogenesis of heart failure [30, 31].

β_1-AR stimulation influences the heart contraction rate more than β_2-ARs [29, 32] with a PKA dependent mechanism [33]. Indeed *Devic et al*. examined CM contraction rate in presence of a PKA inhibitor in CM isolated both from β_2-AR KO mice and from β_1-AR KO mice. They observed a small increase in CM activity in the β_2-AR KO CMs compared to the β_1-AR KO ones, suggesting that the β_1-AR pathway is PKA dependent [33].

The two receptor subtypes have also different distribution in the cell surface: by using scanning ion conductance microscopy (SICM) with measurements of cAMP production by using FRET-based approach, it has been shown that selective activation of β_1-AR in isolated adult CM was achieved by stimulating the cell crest areas, on the contrary activation of β_2-ARs was obtained stimulating the T-tubular region [34]. Moreover the response mediated by the β-ARs triggers different compartmentalization of the intracellular cAMP. FRET-based measurements in adult CM show that β_1-AR selective activation induces intracellular cAMP increase that diffuses through the entire cytoplasm, instead β_2-AR-mediated signal remain restricted to local domains.

The control of the selective β-AR mediated cAMP increase is modulated by different PDEs, β_1-ARs cAMP signal is controlled especially by PDE4, on the contrary β_2-AR pathway is controlled by multiple PDE isoforms [35].

It has been demonstrated that in patients affected by heart failure occurs an increase in the plasma concentration of NE due to the over activation of sympathetic nervous system [36], and this could lead to a desensitization in the β-ARs, in particular it has been shown that in pacing-induced heart failure in dogs occurs a downregulation of β_1-ARs before the developing of the heart failure [37]. In line with these data, there is evidence of a reduction of mRNA level of β_1-ARs in failing heart biopsy, and this decrease is correlated with the

severity of the disease [38]. Considering that it has been demonstrated that β_1-AR are enriched in the region of the heart that interact with a sympathetic neurons [3], β_1-AR downregulation could be involved in a disruption of a SN-CM specialized interacting site that modulates heart rate during stress or exercise.

Taking into account this consideration it becomes important to understand whether autonomic regulation of cardiac performance through β-ARs occur by specialized interaction between SNs and CM or by a non-structured connection, in order to investigate the pathophysiological role of SNS in arrhythmia triggering.

5. FRET Measurements of cAMP and PKA activity in living cells

To monitor cAMP variation and PKA activity in the cytoplasm of living cells become important in order to assess CM intracellular signaling upon β-AR stimulation with high temporal resolution. In the last few years FRET-based biosensors were developed. In this work we used two different FRET-based probes: EPAC1-camps and AKAR3, to monitor cAMP increase [39] and PKA activity, respectively [40]. FRET (Förster resonance energy transfer) is an event that describes a transfer of energy between two chromospheres. A donor chromophore which is in the excited state may give a part of the energy to excite the acceptor chromophore. The efficiency of the transfer depends on chromophores orientation, on the acceptor-donor distance and on fluorophore spectra that have to be overlapped. This property of the fluorescence protein was applied to build up genetic encoding probes to monitor intracellular messengers variation in living cells.

EPAC1 is a protein which is activated by cAMP [41] produced by β-AR stimulation. EPAC1 was fused with two fluorescence protein suitable to making FRET (CFP, donor and YFP, acceptor) [39] and it is expressed in cells by transient transfection. When the intracellular concentration of cAMP is low, EPAC1 is not activated and the two chromophores are one close to the other inducing high FRET signal. When intracellular cAMP increase, EPAC1 is activated and undergoes conformational changes, augmenting the distance between the two chromophores, with a decrease in the FRET signal [39] (**FIG 3**). cAMP variation is measured as ratio between the fluorescence intensity of CFP and the fluorescence intensity of YFP.

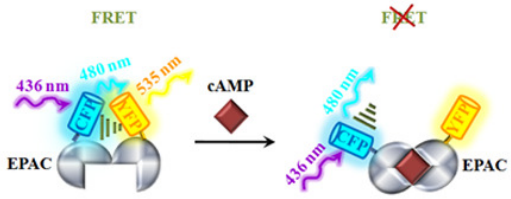

Figure 3 : Schematic representation of the FRET-based biosensor EPAC1-camps. EPAC is a physyological target of cAMP. It was fused with two fluorescent protein (CFP and YFP). In presence of low concentration of cAMP CFP and YFP are one close to the other triggering high FRET signal. When cAMP concentration increase EPAC changes its conformation, increasing the distance between the two fluorophore and conversely decreasing FRET signal.

AKAR3 biosensor detects PKA activation by cAMP. AKAR is a four part chimeric protein made of CFP, a phospho-amino acid binding domains, a PKA specific phosphorylatable sequence, and YFP [40]. When PKA is deactivated the distance between CFP and YFP is high and there is no transfer of energy between the two fluorophore; cAMP-activated PKA phosphorylates the target sequence of the biosensor changing its conformation interacting with the phospho-amino acid binding domains; in this way the distance between CFP and YFP decreases and the energy trasfer can occurs [40] . PKA activity is assessed as ratio between the fluorescence intensity of YFP and the fluorescence intensity of CFP [40].

AKAR biosensor was improved by changing the fluorescence protein: a pair of yellow and cyan fluorescence protein, CyPet and Ypet was fused. Indeed CyPet and Ypet are optimal FRET pair, that gives higher FRET efficiency than other chromophores couples[42]. This improved FRET-based biosensor is AKAR3 (**FIG 4**).

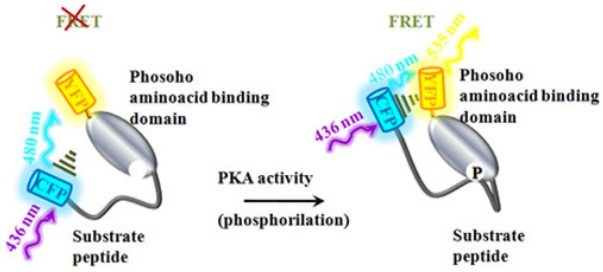

Figure 4 : Schematic representation of the FRET-based biosensor AKAR3. AKAR3 biosensor is a reporter of PKA activity. It is made of CFP, a phospho-amino acid binding domains, a PKA specific phosphorylatable sequence, and YFP. When PKA is deactivated the distance between CFP and YFP is high and there is no transfer of energy between the two fluorophore; cAMP-activated PKA phosphorylates the target sequence of the biosensor that change its conformation interacting with the phospho-amino acid binding domains; in this way the distance between CFP and YFP decreases and the energy trasfer can occurs

With these biosensors we were able to monitor both cAMP variation and PKA activity in living cells to investigate β-AR intracellular signaling triggered by sympathetic neurons (SN).

Plasmid encoding for EPAC1 or AKAR3 were expressed in plated-cells by transient transfection. Cells were rinsed and maintained in a Ringer-modified saline (for FRET recording. Cells were imaged on an inverse fluorescent microscope (IX50, Olympus) coupled to a CCD camera (Sensicam QE, PCO) and a beam-splitter optical device (Microimager) (**FIG. 5A**).

Coverslips with cells attached were put onto the objective. FRET intracellular variations were recorded during time with high temporal resolution. Cells expressing FRET-based probe were excited at 436 nm (CFP). The emitting light (CFP and YFP signal) was split in two channel by a beam splitter device, and two image (CFP and YFP) are detected by a CCD camera and transferred to a dedicated computer using custom-developed software (Roboscop) (**FIG. 5B**).

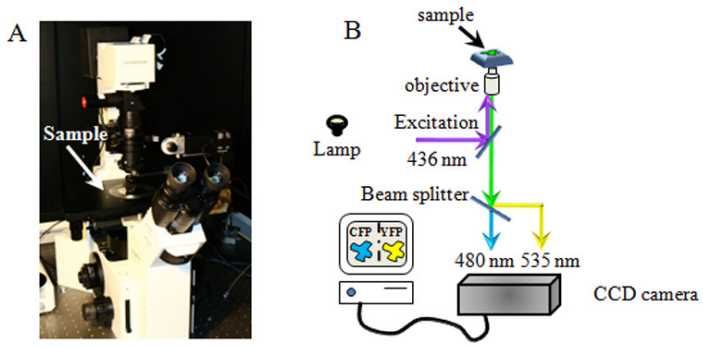

Figure 5 : Schematic representation of fluorescent microscope setup. A. Setup for live cells FRET imaging. **B.** A typical set up is formed by a inverted fluorescent miocroscope that was connected to a CCD camera a beam-splitter optical device, and a light saurce for CFP excitation (436 nm). Coverslips with cells attached were put onto the objective. FRET intracellular variations were recorded during time with high temporal resolution. Cells expressing FRET-based probe were excited at 436 nm (CFP). The emitting light (CFP and YFP signal) was split in two channel by a beam splitter device, and two image (CFP and YFP) are detected by a CCD camera and transferred to a dedicated computer using custom-developed software (Roboscop).

After PKA activation the ratio YFP/CFP displayed increases, on the contrary after EPAC1 activation the ratio YFP/CFP displayed decreases. FRET values were expressed as $\Delta R/R_0$, where R_0 is the ratio at t = 0 s and $\Delta R = R - R_0$.

6. *In vitro* and *in vivo* evidence of specialized interaction between SN and CM

The heart is densely innervated by sympathetic neurons that regulate cardiac function during exercise and stress through β-ARs activation. To date, whether the sympathetic neurons interacts with the cardiomyocytes with a direct cell-cell interaction or if the autonomic control of the heart is mediated by diffuse release of catecholamines in the tissue not specific, is still elusive.

A suitable in vitro model to study sympathetic neruons-cardiomyocytes interaction is represented by SN-CM co-cultures. There are studies in which a close interaction between SN and CM has been suggested. Electron microscopy analysis (EM) on SN-CM co-cultures showed presence of varicosities containing synaptic vesicles along the axons at 20-30 nm from the myocyte surface [43], and there is evidence that electrical stimulation of SN induces an increase in the contraction rate in co-cultured CMs[3, 44-46] due to NE release from catecholamine-releasing terminal interacting with the ventricular myocytes [46]. *Marvin et al.* in 1984 performed co-cultures between sympathetic chain explants with isolated ventricular myocytes, observing that axons migrated from the sympathetic chain tissue interacts with ventricular cells avoiding the connection with the non muscle cells. To verify the functional connection between those neurons and the cardiac cells they monitored the CM beating rate upon nerve stimulation, showing increase in the contraction frequency in co-cultured CM [47].

This evidence is supported by the fact that electrical stimulation of SN induces variation in the electrical properties of the coupled-cardiac cells *in vitro [48]*, and that NGF treatment elevates spontaneous beating rate of the coupled-cardiac cells [22], implying that the innervation is functional and cardiac specific.

In accord with this hypothesis, it has been demonstrated that sympathetic innervation influences protein expression and localization of the co-cultured CMs. Indeed SN innervation lead to an increase in the L-type Ca^{2+} channel expression [46], that is essential in the myocyte contraction during the CICR event, and β_1-ARs were enriched in specialized zone that surround contacting axon, in close proximity of scaffold protein such as AKAPs and SAP97 [3]. All these data support the hypothesis of existence of a specialized site that modulates cardiac activity by releasing NE that interacts with the post-synaptic β-ARs.

A model in which autonomic control of contractility occurs through direct interaction between the neurons and their target CM could be also suggested by the fact that impairment in the SNS function could lead to arrhythmias [49], supporting the idea of the existence of specific interaction between SNS and heart. First of all, it has been demonstrated that unbalanced sympathetic input of cardiac innervation is involved in the arrhythmic events [50]. Indeed it has been observed that the autonomic innervations in dog affected by inherited arrhythmias have a heterogeneous distribution: there were area of denervation in the apical, anterior, septal, and lateral regions of the left ventricle [50]. The connection between unbalanced sympathetic innervations and the arrhythmias triggering is also supported by the fact that patients affected by ventricular arrhythmias have a sustained activation of the sympathetic nervous system [49] and after myocardial infarction (MI) sympathetic innervation increased in the peri-injured area [27, 51] with upregulation of several growth factor such as Nerve Growth Factor (NGF) [51] and disappeared in the necrotic area [27, 51]. Thus, MI-induced nerve growing created heterogeneous distribution of the sympathetic innervation, with hyperinnervated, denervated areas and normal nerve fiber density [51].

Therefore considering that MI leads to VT-related hyperinnervation and heterogeneous sympathetic nerve distribution that is involved in arrhythmia triggering, it has been suggested that SNS impairment is involved in the genesis of arrhythmic event in diseased hearts.

Moreover it has been demonstrated that, in isolated and perfused heart with chronic MI and failure, it has been shown that the proarrhythmic input is sympathetic nerve stimulation, that triggers a β-AR-mediated arrhythmic event [52], that could be originated by hyperactivation of SNS also in patients without conventional risk of sudden cardiac death [53].

Sympathetic nerve stimulation in failing myocardium leads to the release of NE through nerve endings, thus hyperactivation of SNS could increase the release of NE. These events support the evidence that NE spillover in the plasma occurs in patients with heart failure [36, 37], due to impairment in the SNS function caused by unbalanced hyperactivation of sympathetic nerve or failing in the NE reuptake by norepinephrine transporter (NET).

Indeed it has been proposed a significant reduction of NE-analog (MIBG) uptake in patient with idiopathic ventricular fibrillation [54], and $NET^{-/-}$ mice show increase in the

plasma NE with increase in the heart rate [55], as occurs in patients with failing myocardium condition, suggesting a possible trigger mechanism for arrhythmic events. In addition, *Myles et al.* recently provided evidence that NE stimulation of small fraction of cardiac cells is sufficient to trigger a premature ventricle complex in isolated and perfused heart[56], raising the hypothesis that β-local adrenergic activation is involved in triggering arrhythmic event in pathophysiological states, and such dysfunction leads to the activation of a limited fraction of cardiac cells sufficient to generate premature beat in the whole heart.

These data support a model in which autonomic control of small fraction of cardiac function relies on specialized interaction sites of direct interaction between the neurons and their target CM.

The autonomic stimulation of the heart during exercise or stress condition is a trigger mechanism also in stress-related inherited arrhythmias, such Cathecolaminergic Polymorphic Ventricular Tachicardia (CPVT). Thus, become important to understand whether the sympathetic nerve fiber control a limited group of cells, in order to understand which the fraction of CPVT-cardiac is cells that have to be depolarized o trigger the arrhythmic event.

7. Cathecolaminergic Polimorphic Ventricular Tachicardia (CPVT)

CPVT is inherited arrhythmia that leads to syncope and sudden death during stress or exercise. Electrocardiography analysis on patients without any conventional risk of sudden death, affected by CPVT is characterized by stress-related ventricular tachycardia (VT), leading to fibrillation or cardiac arrest. To date the only therapeutic strategy is the use of β-blockers, but 30% of the treated-patients develop strong VT [57].

There are two genetic variants of CPVT: autosomal dominant form, caused by the mutation of the gene coding for Ryanodine receptor2 (RyR2) [58], and autosomal recessive form, caused by the mutation of the cardiac isoform of Calsequestrine2 (CASQ2) [59] . The autosomal-dominat form of CPVT is characterized by missense mutations in RyR2. However the molecular mechanism involved in the arrhythmias triggering is debating (**FIG. 6**).

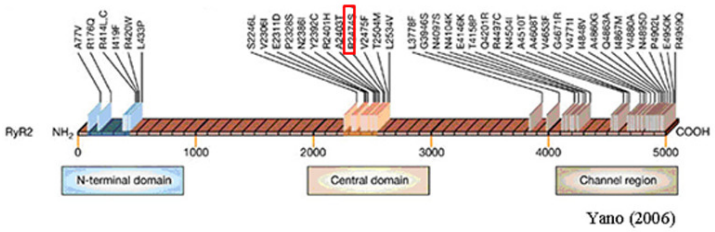

Figure 6: Scheme of mutation of the gene enconding for CPVT-linked RyR2. The autosomal dominant form of CPVT is connected missense mutations of RyR2. Several mutations have been identified but the most common one is the R2474S

During exercise or stress condition heart increase the beating rate by the release of NE from SNS that interacts with β-AR activating PKA through cAMP pathway. PKA activation induces phosphorylation of several proteins , in particular RyR2 [25]. RyR2 is a Ca^{2+} permeable channel localized in the membrane of sarcomplasmic reticulum (SR), that upon phosphorylation shift in a open conformation allowing the passage of Ca^{2+} from SR lumen to cytosol increasing intracellular Ca^{2+} availability to cardiac contraction [60].

PKA phosphorylation triggers displacement of a protein, Calstabin2 (FKBP12.6), that keep the channel in the close state, increasing the open probability (P_o) of the channel [61]. *In vivo* and *in vitro* studies have been shown that RyR2-linked CPVT decreases the affinity to Calstabin2 in PKA-mediated phosphoryaltion state [62, 63]. As consequence RyR2-CPVT P_o is higher than in wt RyR2 in presence of low concentration of cytosolic Ca^{2+} (during dyastole) [62]. Thus a leakage of Ca^{2+} from SR occurs in CM also during diastole leading to activation of the NE^{+}/Ca^{2+} exchanger (NCX), that reduce the membrane potential to the threshold potential to activate NE^{+} channel, triggering a premature beat during diastole[64]. Thus the leakage of Ca^{2+} from mutated-RyR2 causes membrane potential instability that could lead to arrhythmic events.

In other study RyR2 mutation linked to CPVT increase the store overload-induced Ca^{2+} release (SOICR)[65], an event in which the increase in the SR luminal Ca^{2+} induce spontaneous leakage of Ca^{2+} by RyR2. In support to FKBP12.6-indipendent mechanism there are *in vitro* studies showing that the dissociation between FKBP13.6 and RyR2 does not cause the CPVT-phenotype[66]

These different interpretations of triggered arrhythmias in CPVT, could also change the strategy on developing molecular approaches to correct functional defect, thus it becomes important understand the pathophysology of CPVT that is not completely clear.

Patients affected by CPVT at ECG analysis has normal heart structure and normal QT interval [67]. During the arrhythmic event they show ventricular extrasystole following by bidirectional ventricular tachycardia that could degenerate into ventricular fibrillation[67]. It implies that the arrhythmic events originate from an irregular activity of a limited group of cells, thus it becomes important whether the increase in the P_0 of RyR2 of a small group of cardiomyocytes is sufficient to trigger VT events.

In a part of this project we set up a channelrhodopsin2-based mouse model to investigate which is the fraction of cells that have to be depolarized to trigger an arrhythmic event both in normal condition and in CPVT condition, and understand the role of SNS in the VT triggering.

8. Channelrhodopsin2 (ChR2)-based approaches to modulate exitable cells activity

ChR-microbial proteins are light-gated cation channels localized in the plasma-membrane of the cells. They are rhodopsin-like proteins with a seven transmembrane domain that undergoes conformational changes upon absorption of photon[68], allowing the passage of the ion within the channel (**FIG.7**).

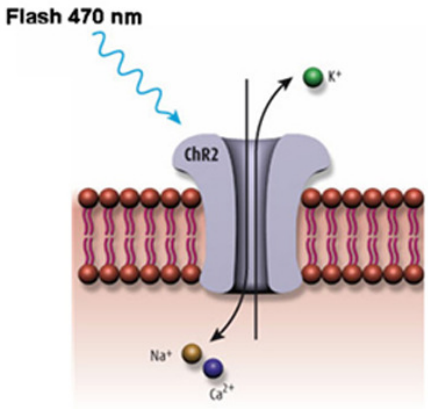

Figure 7: Activation scheme of the light-gated protein ChR2. ChR2 is a light-gated cation channel that pecome permaeable mostly to Na^+ upon light stimulation at 470 nm.

The wavelength to trigger the activation, the ion selectivity and conductance differ among the ChR-variants [68]. In this work we used ChR2 which is a variant of the ChR protein that is part of phototactic apparatus of algae *Chlamydomonas reinhardtii[69]*. ChR2 activation upon blue light (470 nm) triggers a conformational change that allows the passage of Na^+ with millisecond resolution [4, 68].

ChR2 has successfully been used to modulate neuronal circuits with light pulses[4, 5, 70, 71] or to control neurons activity in brain slices[72]. Indeed it has been demonstrated that ChR2-positive neurons in cortical slices triggers rapid current sufficient to elicit an action potential[72]. This ChR2 property has also been shown in the entire brain, in fact Deissand co-workers induced expression of ChR2 in the motoneurons and using a 200µm fiber optic they were able to modulate mouse behavioral in a non-invasive and time-controlled way[72] and to map neural circuits in the brain [73].0

Thus ChR2 stimulation with blue light induces a depolarization sufficient to trigger an action potential in neuronal cells and it is useful to fast-modulate brain activity and behavior of living animals.

ChR2-based approach is suitable to modulate the activity of other excitable cells. Indeed this novel approach is applied also to control cardiac cells activity, modulating by light both electrical properties of cardiac cells obtained by stable transgenic mouse embryonic stem cell line expressing ChR2(H134R) and electrophysiological behavior of the heart[74]. ChR2 become a useful tool to control cardiac activity in *vitro* and *in vivo,* allowing to stimulate a limited number of cells in the heart. Thus this strategy let us depolarize the heart in different region of decreasing size to understand the fraction of cells that have to be depolarized to trigger an arrhythmic event.

Aims of the project

The data here presented suggest that SN innervation of the heart determine a specific and regulated domain with the target cells. Indeed EM analysis on SN-CM co-cultures showed that SN interacts closely with the CM forming organized structure where ST interacts with the cardiac cells[43]. Moreover it has been shown that SNS overactivation is involved in the trigger mechanism of heart failure and arrhythmic event in physiological and pathophysiological condition, such as MI [49, 51]. Impairment in the sympathetic nerve electrophysiological properties lead also to NE spillover in patients with history of tachiarrhythmias or heart failure[36], due also to an impairment in the NET function[54]. Increase in the NE concentration is suggested to be one of the trigger mechanism of arrhythmic events, and local administration of NE is sufficient to trigger a premature beat [56].

All the evidence here provided supports a model in which the autonomic control of the heart occurs in a specialized synaptic site in which NE is released controlling CM intracellular signaling. Taking into account all this consideration we made the hypothesis that impairment of autonomic innervations could caused a variation of electrical properties of a limited group of cells sufficient to trigger a premature ventricle beat.

Thus the aims of this project are:

1. To investigate whether specific cell-cell interactions have a role in the dynamics of intercellular signaling between SN and CM.
2. To understand whether the unbalanced SN modulation of a limited group of cardiac cells could be involved in generating arrhythmias *in vivo* using a ChR-based strategy.
3. To study *in vivo,* non-invasively, the critical mass of myocardium necessary to generate an arrhythmogenic focus based on a ChR2 approach.

In Chapter 1 I will provide evidence of the existence of a SN-CM specialized and restricted releasing site, using an *in vitro* model. To provide also this evidence *in vivo* in chapter 2 I will describe a bioinformatic model of ChR2 that allow to understand the

structure of the protein, adding preliminary results that show how ChR2 based strategy allow to control the neuronal-like cells behaviour *in vitro* and also SN activity *in vivo.*

Finally in chapter 3 I will show a novel system to optically control heart activity in normal condition or during pro-arrhythmic condition, showing the critical mass necessary to trigger a premature ventricle beat. This work is currently ongoing, and we are performing additional experiments to increase the trial number. The results of the present discussion constitute one manuscript currently in submission, one in preparation and one published. Each of these pieces of work will appear in separate chapters.

Live imaging of the neurocardiac signaling interaction

Abstract

The heart is densely innervated by sympathetic neurons that regulate cardiac function during exercise and stress through β-ARs activation. Unbalanced sympathetic discharge to different regions of the heart has been associated with arrhythmia triggering [1], and alterations in presynaptic NE reuptake lead to catecholamine spillover in the failing myocardium [2]. These data support a model in which autonomic control of contractility occurs through direct interaction between the neurons and their target cardiomyocytes (CM).

The aim of this study is to investigate whether specific cell-cell interactions have a role in the dynamics of intercellular signaling between autonomic neurons and CMs *in vitro*.

Intracellular β-AR-dependent signaling was assessed in intact neonatal rat CM co-cultured with superior cervical ganglia neurons (SN) by performing real-time cAMP and PKA activity imaging upon SN stimulation with KCl or bradykinin.

In co-cultures SNs extend their axons upon NGF treatment and establish direct contact with CM. Activation of a specific SN lead to cAMP increase in the interacting CM while no changes in cAMP were detectable in neighbouring but not directly interacting CMs.

To assess the [NE] that interact with the post-synaptic β-ARs we set up a pharmacological assay using the non-selective β-blocker propranolol. We observed that 10e-5 M of propranolol totally inhibits the cAMP increase induced by neurotransmitter released from SN. The same concentration of propranolol inhibits the response elicited by 10e-7 M of NE administered to CM plated alone, suggesting that the [NE] acting in the synaptic cleft is in the order of 100 nM.

Here we provide evidence of a 'synaptic' contact between SNs and CMs that form a high agonist concentration, diffusion-restricted space allowing potent activation of a small fraction of β-AR on the CM membrane upon neuronal stimulation.

Introduction

Cardiac sympathetic neurons modulate heart activity by increasing the force and the frequency of heart contraction, mediating the response known as *'fight or flight response'*. This suggests that a function coupling exists between these cells.

Indeed, efforts have been performed since the late 70s to study such cell-cell interaction in vitro. Electron microscopy analysis (EM) on neonatal cardiomyocyte and sympathetic neuron co-cultures showed the presence of varicosities containing synaptic vesicles along neuronal axons 20-30 nm from the myocyte surface [3]. Electrical and pharmacological stimulation of SNs modifies the electrical properties of the coupled-cardiac cells *in vitro* [4] and an increase in the contraction rate in co-cultured CMs [5-8], as well as electrical stimulation of the sympathetic ganglia explants induces a positive chronotropic response in co-cultured ventricular myocytes [9].

Dysfunction of the sympathetic nervous system is implicated in several cardiovascular diseases, including arrhythmias and heart failure. Heterogeneous distribution of cardiac innervations is involved in the arrhythmic events [10]. Patients affected by ventricular arrhythmias have sustained activation of the sympathetic nervous system [11], leading to increase in the released NE. Indeed there is evidence that NE spillover in the plasma occurs in patients with heart failure [12, 13].

Ripplinger and coworkers recently provided evidence that NE stimulation of a small fraction of cardiac cells is sufficient to trigger a premature ventricle beat in the isolated and perfused heart [14], raising the hypothesis that SNS impairment is involved in the triggering of arrhythmic event, and such dysfunction leads to the activation of a limited fraction of cardiac cells sufficient to generate a premature beat in the whole heart.

All this evidence supports a model in which the autonomic control of the heart occurs in a specialized site in which NE is released controlling CM intracellular signaling.

The existence of specialized sites has been demonstrated for the neuromuscular junction (NMJ), where high concentration of neurotransmitter binds to postsynaptic membrane receptors accumulated in the synaptic site together with channels, anchoring and signaling proteins required for muscle contraction [2].

SNs exert their function by releasing norepinephrine (NE) from nerve endings, leading to activation of cardiomyocyte beta-adrenergic receptors (β-ARs). This activates adenylil cyclase producing the second messenger cyclic AMP (cAMP) and leading to activation of PKA in the cAMP/PKA pathway. PKA mediates its functional effect by phosphorylating several cytoplasmic and nuclear targets involved in the increase in force and frequency of heart contraction. Thanks to many FRET-based biosensors developed in the recent years, it has been possible to monitor cAMP variations in real time in living cells, highly improving the knowledge of intracellular cAMP dynamics in cardiomyocytes.

Given the growing evidence that localization of signaling events in the CM plays a role in cardiac physiology and pathology, uncovering the mechanism of neurocardiac regulation is of paramount importance.

We sought here to develop an *in vitro* model to mimic the interaction between sympathetic neurons and cardiomyocytes allowing the study of the physiological β-AR activation in CM cAMP/PKA signaling. We set up co-cultures between neonatal rat CM and superior cervical ganglia neurons. We performed real-time cAMP and PKA activity imaging with the FRET-based biosensor EPAC1-camps and AKAR3, respectively, in CM coupled with SN.

Results

Co-cultures between cardiomyocytes and sympathetic neurons as an *in vitro* model to study cell-cell interaction and intercellular signaling.

The sympathetic nervous system represents the fundamental modulator of cardiac activity, regulating heart rate, conduction velocity and myocardial contractility through the release of catecholamine and activation of β-adrenergic receptors (β-ARs). The evidence describing the role of β-ARs in regulating the intracellular signals controlling myocardial function has been so far accrued on isolated cellular preparations, in most cases with exogenous pharmacological receptor stimulation. Sympathetic neurons activation, however, is the main mechanism whereby the β-ARs are stimulated in the living organisms. Although the distribution of cardiac sympathetic neurons (SNs) is well established, and so is the mechanism leading to catecholamine release, it is currently unclear whether a specific cell-cell interaction between SNs and their myocardial targets exists.

We have established an *in vitro* model to mimic the physiological interaction between SNs and cardiomyocytes (CMs) by setting up co-cultures of neonatal rat neurons isolated from the superior cervical ganglia and ventricular CMs.

Myocytes and SNs were cultured on the same coverslip and kept in 2^{nd} day medium supplemented with 100 ng/ml of NGF. After 1 week in culture, SNs have developed axons that take contact with several CMs [15, 16] (**Figure 1A, and B).** This situation mirrors the condition *in vivo*, where a dense pattern of cardiac sympathetic innervation is present, as shown for ventricular cryosections of adult mouse hearts stained with an antibody to synapsina 1a (, **FIG.** 1**D**). Immunofluorescence analysis reveals that a close interaction of single actively-releasing neurons with different cells exist, as presented in ventricular cryosections from adult mouse hearts where the CM membrane is stained with FITC-conjugated wheat germ agglutinin and neurotransmitter-releasing sites are depicted with an antibody specific for synapsina 1a (**Figure 1 C).**

In co-cultures, accumulation of synapsinI in the pre-synaptic membrane (**Figure 1C**) and β-catenin and cadherins in the CM membrane was observed at the site of contact [6] (and data not shown).

These results indicate that in our co-cultures specialized connections form between the two cell types and that our system is feasible for studying the intercellular signaling between SNs and CMs.

Intracellular cAMP dynamics in cardiomyocytes coupled to sympathetic neurons upon neuronal activation.

To investigate whether the CM-SN synaptic contact is functional, we set out to measure intracellular cAMP levels in CMs coupled to SNs by expression of the cAMP FRET-based biosensor Epac1-camps in CMs prior to co-culture establishment (**FIG. 2A**). This sensor reports on cAMP levels by monitoring FRET between CFP and YFP fused to the cAMP binding domain of an isoform of the exchange protein directly activated by cAMP[17] (Epac1). Accumulation and subsequent binding of cellular cAMP induces a conformational change that decreases the FRET efficiency between the two fluorescent proteins. Therefore, the ratio between CFP and YFP emission is proportional to the concentration of intracellular cAMP ($[cAMP]_i$).

SNs were stimulated by applying high potassium solution (50 mM) to the cell bath, followed by washout with saline solution (5 mM K^+). This treatment causes the onset of a train of action potentials and direct membrane depolarization that stabilizes to a membrane potential of about 0 mV that lasts as long as high KCl is present (**Fig. 2B**), and subsequent rapid intracellular calcium increase (**FIG. 2C**) by influx through voltage-gated calcium channel. This event is necessary for the exocytotic release of norepinephrine (NE).

Under this condition, SN depolarization induced an increase in $[cAMP]_i$ in innervated CMs. In **FIG. 2D**, a representative trace of CM $[cAMP]_i$ monitored as increase in the ratio between the 480 nm/535 nm emission signals (R) over the value at t = 0 s (R_0) is illustrated. The graph also shows the increase in $[cAMP]_i$ upon 1 nM and 10 nM NE administration to the cell bath in the same cell, used to monitor for single cell health and responsiveness. In CMs contacted by SNs, the increase in $[cAMP]_i$ upon 50 mM KCl stimulation was higher ($\Delta R/R_0$ = 5.61 % ± 0.01 mean ± SEM, n = 8) in comparison to myocytes in co-culture but without synaptic contacts and myocytes cultured alone ($\Delta R/R_0$ = 1.70 % ± 0.01 mean ± SEM, n = 12) (**FIG 2E, 2F**). The fact that in CMs in co-culture but without sympathetic contacts $[cAMP]_i$ increase was not observed indicates that this

effect is specific and not simply due to NE released into the medium by simultaneous depolarization of all SNs in culture. Synapse formation was confirmed by incubating the cells with FM1-43 (not shown).

To further exclude the possibility that the increase in CM $[cAMP]_i$ could be caused by unspecific release of NE in the medium by depolarized SNs, we puffed high potassium solution specifically to the SN coupled to the CM under observation. This was achieved via positioning the tip of a picospritzer pipette in proximity to the SN and applying a pressure of 5-10 psi for up to 10 s.

To verify that the puff is sufficient to induce depolarization SNs were loaded with Fluo4-AM and intracellular calcium increase with was monitored.

A brief puff of KCl (5 psi, 10 s) delivered to the soma induced a rapid increase in intracellular calcium in SNs ($t_{1/2}$ = 1.23 s ± 0.33, mean ± SEM, n=4) (**FIG. 3A**).

Using the same protocol e measured intracellular cAMP variation in innervated CM. we observed that brief KCl puff induces increase in $[cAMP]_i$ ($\Delta R/R_0$ of 1.724 % ± 0.003, mean ± SEM, n = 3) was detected (a representative trace is shown in **FIG. 3B**).

The comparison of calcium dynamics in SNs and cAMP increase in CMs shows that cAMP production starts about 2 s after the increase in intracellular calcium and is at about half of its peak when calcium concentration is at its maximum

In about 15% of the CMs analyzed, high potassium administration induced a transient increase in $[cAMP]_i$ with $\Delta R/R_0$ of 6.59 % ± 0.008 (mean ± SEM, n= 2).

Our results indicate that a functional synaptic contact form between SNs and CMs in co-culture, whereby single SN activation can specifically control the intracellular signaling of coupled CMs, possibly via β_1-ARs.

This evidence is also supported by the fact that structural organization occurs in the CM membrane under ST, in particular that β_1-ARs are enriched in the region of SN-CM contact [6]. Using β-ARs subtype tagged with a HA (β_1-ARs) or flag (β_2-ARs) we verified receptor localization in our model. **FIG. 4A** represent a confocal image of SN interacting with CM expressing β_1-HA. In contacting region (indicated with the arrows) we observed accumulation of the receptor, on the contrary in non-interacting region the expression of the receptor is lower. Instead β_2-ARs are evenly distributed on the plasmamembrane of CM, also in the interacting region (**FIG. 4B**).

These differences in the localization allow us to think that neurocardiac coupling is mostly β1-AR mediated. Thus we performed the functional assay previous described in presence of selective β-ARs blockers. We observed that the SN-induced cAMP response in presence of β_1-AR blocker (CGP 12177A, 50 nM) is lower to that induced in presence of β_2-AR blocker (ICI 118511, 40 nM), confirming the fact that SN control XM activity mainly via β_1-ARs (**FIG 4C**). In conclusion these results indicate that the specific neurocardiac regulation occurs possibly via β_1-AR.

Quantification of the SN-released NE in the synaptic cleft

It has been demonstrated that SN influence CM contraction rate [6, 7], and here we have provided evidence that such interaction is specific and determines a domains in which NE is released activating mostly β_1-ARs.

To understand which is the NE concentration acting in the synaptic cleft we compare the variation of the FRET ratio of EPAC1-camps raised from administration of different concentration of NE given to the bathing solution to that elicited by SN-released NE ($\Delta R/R_0$= 2.6 % ± 0.6%, mean ± SEM, n=13).

We measured the effect of NE as percent of maximal response (**fig. 5A**). The variation in the CFP/YFP ratio induced by SN-released NE (2.6%) is comparable to that induced by 3.5e-10 M of NE administered to the whole cells (FIG**. 5A dotted line, 5B**).

However, sympathetic-releasing terminal interacts with a limited fraction of the membrane of the coupled-CM, so the cAMP increase achieved by SN-released NE is due to a stimulation of a small number of high-density receptor. On the contrary cAMP variation elicited by exogenous administration of NE is triggered by stimulation of β-AR distributed on the plasmamembrane, implying that the β-AR activation induced by SN-released NE is triggered by high concentration of neurotransmitter that activate a limited but high receptor density fraction of the membrane of the coupled CM.

To assess the [NE] that interact with the post-synaptic β-ARs we set up a pharmacological assay using the non-selective β-blocker propranolol. Propranolol is a competitive antagonist of NE, meaning that at increasing concentration, propranolol competes with SN-released NE in the β-AR receptor site until the response is abolished. We standardized the amount of NE released from SN by stimulating the sympathetic nerve for a fixed

period of time (15 s). In this way we have a model in which the unknown amount of NE discharged is stable and the concentration of antagonist is changed in order to understand which is the amount of β-blocker needed to completely abolish the response triggered by SN-released NE. We observed that low concentrations of propranolol (100 nM, 200 nM9 do not inhibit the response induced by SN, but are sufficient to abolished the response triggered by 3.5e-10 M of NE (**FIG 5B**) confirming the hypothesis that NE acts in a limited fraction of the membrane activating high-density receptor.

We build up a dose response curve of NE in presence of propranolol and we observed that 10e-5 M of propranolol totally inhibits the cAMP increase induced by neurotransmitter released from sympathetic nerve endings (**FIG. 5C**).

We performed the same experiment by administering a known concentration of NE to CM plated alone in presence of increasing concentration of propranolol.

We found out that the response elicited by 10e-7 M of NE given to all the receptor is totally abolished by 10e-5 M of propranolol (**FIG 5D**).

These data show that the response achieved by NE released from sympathetic neuron endings is abolished with the administration of 10e-5 M of propranolol which is the concentration needed to inhibit the cAMP increase triggered by 10e-7 M of NE. This implies that the concentration acting in the synaptic cleft is in the order of 100 nM.

Material and Methods

Sympathetic Ganglion Neuron-cardiomyocyte co-cultures. Primary cultures of cardiac ventricular myocytes (CMs) were prepared from 1- to 2-day-old Sprague Dawley rats as previously described. Briefly, hearts were removed, minced in ADS (106 NaCl, 5.3 KCl, 20 Hepes, 0.8 Na_2HPO_4, and 0.4 $MgSO_4$, in mM) and enzimatically dissociated with collagenase A (0.4 mg/ml) (Roche) and pancreatine (1.2 mg/ml) (Sigma). Sympathetic neurons (SNs) were isolated from 1- to 3-day-old Sprague Dawley rats by adapting the procedure of Zareen and Greene [Zareen, 2009 #1]. Both superior cervical ganglia were minced in complete medium (RPMI supplemented with 10% Horse Serum (HS), both Invitrogen) and then enzimatically dissociated in 0.5% Trypsin with no EDTA (Invitrogen) for 30 min at 37°C. CMs and SNs were seeded at a density of 60000 cells/cm^2 and 1500 cells/cm^2, respectively. Cells were plated onto laminin-coated (10 µg/cm^2) round glass coverslips in cardiomyocyte medium (75% D-MEM-Hepes, 17% M199, 5% horse serum, 0.5% newborn calf serum, 200 mM glutamine, penicillin-streptomycin, all from Invitrogen) supplemented with 100 ng/ml NGF (Sigma) and maintained in a humidified atmosphere (5% CO_2) at 37°C. Half of the medium was replaced every two days.
To achieve expression of the FRET-based biosensors in CMs, cells plated on glass coverslips were transfected with Transfectin Reagent (BioRad) following manufacturers' instructions prior to SN plating.

Immunofluorescence on SN-CM co-cultures. SN-CM co-cultures were fixed in 4% paraformaldehyde (PFA) (Sigma) for 30 minutes at 4°C temperature, and processed for immunofluorescence analyses. Cells were permibilized with 0.1% triton-X100 at room temperature, incubated with primary antibodies diluted in PBS supplemented with 1% BSA 2 hours at 37°. The following primary antibodies were used in this study: rabbit anti-flag (1:800, Sigma); mouse anti-HA (1:800, Roche). FITC- and Cy3-conjugated secondary antibodies, all from Jackson lab (UK), were used to detect primary antibodies.

Transient transfection of cardiomyocytes. Cardiomyocytes were transient transfected with *TransFectin™ Lipid Reagent* (Bio-Rad). Cells were transfected the day after seeding.

For 6 well plate 3 µg of DNE are put in 250 µl of M199 (GIBCO, invitrogen), incubated 5 minutes at room temperature. Meanwhile 5 µl of transfectine are put in 250 µl M199, and incubated 5 min at room temperature. DNE solution and transfectine solution were combined and incubated 20 minutes at room temperature. Cells were washed once with ADS (106 NaCl, 5.3 KCl, 20 Hepes, 0.8 $NaHPO_4$, 0.4 $MgSO_4$, in mM), and 500 µl of cardiomyocyte medium was added. The DNA-transfectin mix was added drop by drop to the cells and let incubate 4 hours in a humidified atmosphere (5% CO_2) at 37°C.

Fluorescent Resonance Energy Transfer (FRET) measurement. Cardiomyocytes were transfected with a plasmid that express EPAC1 or AKAR3 for 7 days. Cells were rinsed and maintained in a Ringer-modified saline (125 mM NaCl, 5 mM KCl, 1 mM Na3PO4, 1 mM MgSO4, 5.5 mM glucose, 1.8 mM CaCl2, 20 mM Hepes, pH 7.4) for FRET recording. Cells were imaged on an inverse fluorescent microscope (IX50, Olympus) coupled to a CCD camera (Sensicam QE, PCO) and a beam-splitter optical device (Microimager). Images were acquired using custom-made software and processed using ImageJ (National Institutes of Health).

Dual emission ratio was acquired with a 436 nm excitation filter, and emission filter (535 nm). The acquisition was set at 500 millisecond of exposure every 5 second of acquisition. Background was subtracted to the images and the ratio of yellow-to-cyan was calculated at different time point. After PKA activation the ratio YFP/CFP displayed increases, on the contrary after EPAC1 activation the ratio YFP/CFP displayed decreases. FRET values were expressed as $\Delta R/R_0$, where R_0 is the ratio at t = 0 s and $\Delta R = R - R_0$.

Discussion

The catecholaminergic neurons innervating the heart are responsible for the continuous adjustment of cardiac performance, through activation of β-ARs, occurring in both the daily activities and in acute stress as part of the *fight-or-flight* response. It is generally accepted that neuro-muscular coupling takes place at multiple interaction sites between the NE-releasing varicosities along the neuronal axon and the target cardiomyocytes. Recent work performed *in vitro* on co-cultures of sympathetic neurons and cardiomyocytes demonstrated that the junctional site between the two cells [6] is characterized by specialization of both the pre- and post-synaptic membranes. However, the functional role of the apposition of the two membranes in signal transmission from the adrenergic neuron to the cardiomyocyte remains largely unexplored.

Here, we used state-of-the art live cell FRET-imaging of cAMP and PKA in sympathetic neuron-cardiomyocyte co-cultures to investigate the dynamics of β-adrenergic signaling at the neuro-cardiac junctional sites. We demonstrate that the synaptic cleft forms a diffusion-limited space allowing NE release to rapidly achieve a concentration sufficient to fully activate β-AR dependent signaling, leading to cAMP elevation and PKA phosphorylation. These results support the concept that neurogenic control of cardiomyocyte function takes place through the direct cell-cell contact, and identifies the neuro-cardiac junction as the unitary functional element in the autonomic control of cardiac performance.

Activation of the cardiac sympathetic neurons enables physiologic enhancement of contractility in response to increased perfusional demand from the tissues. Transmission of the signal from the post-ganglionic catecholaminergic neurons to cardiomyocytes is mediated by NE, which acts on sarcolemmal β-AR. Activation of β-AR increases cAMP synthesis, causing PKA to phosphorylate its downstream targets, including Ca^{2+}-regulating proteins that increase sarcomere shortening rate and force generation.

We implemented co-cultures of sympathetic ganglia neurons and neonatal cardiomyocytes as in vitro model to study the neuro-cardiac signaling axis. Neurons extend their axons in culture and develop multiple varicosities in series that connect with contractile cardiomyocytes (**FIG. 1A**). This model essentially reproduces the morphological features

of cardiac sympathetic neurons, which innervate densely the myocardium and interact with multiple cardiomyocytes as shown in figure (**FIG 1C, 1D**) and in *Zaglia et al.* , Cardiovasc Res. 2013 [18]. Sympathetic neurons in the co-culture exhibited low frequency spontaneous action potentials, as previously reported, and responded to transient membrane depolarization with a rise in $[Ca^{2+}]$ (**FIG. 2B, 2C**). Cardiomyocytes formed a syncytium and had rhythmic spontaneous contractions. We thus used the FRET based biosensors sensing cAMP (EPAC1cAMPs) [17] and PKA activity (AKAR3) [19] to image activation of the β-AR dependent pathway. These biosensors were extensively tested by several groups including ours.

The high spatial resolution of such optical technique allowed assessing signal transmission between the neuron and the coupled cardiomyocytes at the level of the single axonal varicosity and in real time. Stimulation of catecholamine release by a given neuron activated β-AR on cardiomyocytes in contact with the axonal releasing sites, causing a fast and transient elevation in both intracellular cAMP and PKA activity. The neuronal signal was only detected in cardiomyocytes directly interacting with axonal boutons, and was absent in the neighbouring cells (**FIG. 2E, 2F, 2D**). These data indicate that the neuro-cardiac junction is the functional signaling unit of sympathetic neuron/cardiac cell axis. This concept is well supported by the observation that at the junctional site the cardiomyocyte membrane shows clustering of structural proteins and β_1-AR [20] and [Franzoso, ms in preparation], and in agreement with this, the cAMP response evoked by the neuronally released NE was mainly attributable to β_1-AR activation (**FIG. 4C**). It is becoming increasingly evident that β_1 and β_2-AR have a different functional role that is believed to depend on selective distribution of the receptors on the cell membrane [6], causing spatial patterning of intracellular signals, including cAMP [21]. It is tempting to speculate that the selective localization of β_1 AR in proximity to the neuronal release site represent the structural basis ensuring differential β_1-AR *vs* β_2-AR activation by neuronally-released or circulating catecholamines, respectively (27).

We used a propranolol competition-binding assay to estimate [NE] in the cleft, which resulted in the order of 100 nM, indicating that the intermembrane space in which NE is released generates a diffusion-restricted extracellular domain. Thus, thanks to the direct and organized contact, neuronal stimulation leads to activation, at about half potency, of the β-AR pool localized at the junctional site. Ultrastructural definition of the membrane

apposition at the junctional site is outside the scope of the present work, however it has been demonstrated that in cholinergic neuro-muscular junuction, the intermembrane space is in the order of 50-80 nm with only a single layer of basal lamina separating the two structures [22] and we found comparable distances in EM images of co-cultured sympathetic neuron/cardiomyocytes [Franzoso, ms in preparation]. This model has several functional implications: first, the very low volume of the intermembrane space allows to achieve [NE] in the micromolar range with only very few thousands molecules (i.e. few vescicles) released in the cleft; furthermore, this structure allows efficient signaling to the receptors, as supported by simulation models showing that as the minimal distance of the varicosity-to-muscle apposition increases from 50 nm to 200 nm, the number of activated receptors in the post-junctional membrane decreases by about 90% [23]. In addition, direct neuron to cardiomyocyte coupling minimizes diffusion time after secretion of NE, allowing immediate activation of cardiac β-AR responses. This model is in good agreement with the observation that several downstream molecules of the β-AR signaling pathway, including cAMP generating adenylate cyclases, PKA and its targets involved in E-C coupling (i.e. L-type Ca2+-channels) are tethered through scaffold proteins (i.e. AKAPs) in close proximity to the receptor. Interestingly, clustering of such proteins has been observed at the junctional site [6]. Both the efficiency and velocity of signal transmission of the neuro cardiac coupling are unconditional requirements for the beat-to-beat control of cardiac function by the autonomic reflexes.

Dysregulation of the neurogenic control of cardiac function, leading to unbalanced sympathetic input to different regions of the heart, has been correlated to arrhythmia triggering [10]. The concept that sympathetic imbalance has arrhythmogenic potential has been suggested a few decades ago [10] , and demonstrated since then in a number of pathologic states [12, 24, 25]. Regional differences in sympathetic discharge have been associated with arrhythmias in both ischemic hearts and structurally normal hearts of arrhythmic patients. The mechanism whereby regional heterogeneity of sympathetic discharge causes arrhythmia is associated with AP dispersion, an electrophysiological state favouring ventricular arrhythmias. To date, the mechanisms of regional control over cardiac activity by specific groups of cardiac sympathetic terminals are largely unexplored in both physiological and pathophysiological states.

Moreover it has been suggested that stimulation of a limited region of the cells by NE is sufficient to trigger a premature ventricle complex [14], suggesting that the unbalanced SN neurons activity could lead to a depolarization in a limited group of cells that represents the critical mass sufficient to trigger a premature ventricle beat.

FIGURE 1

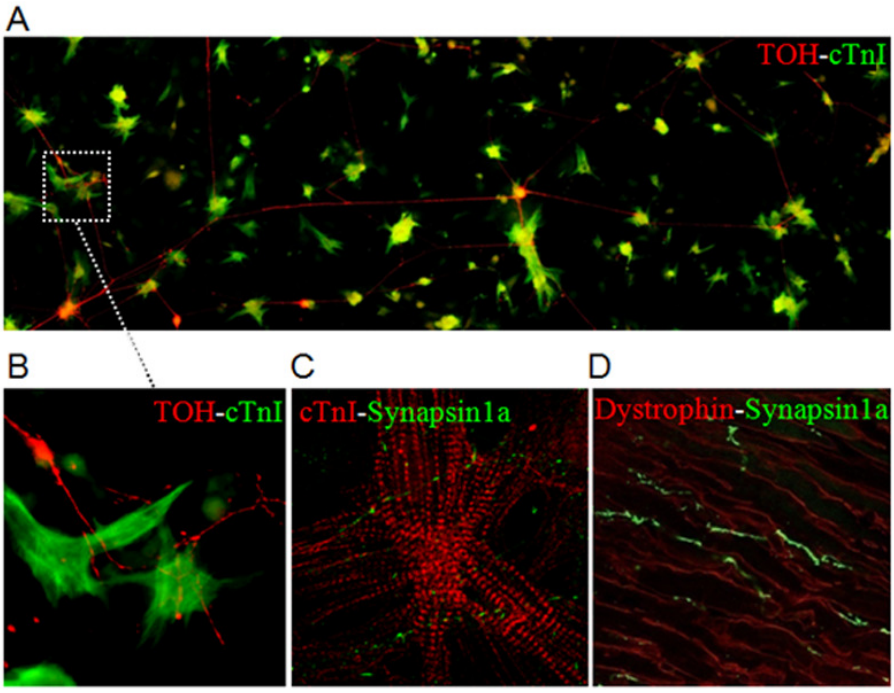

Figure 1

A. SNs isolated from the superior cervical ganglia of neonatal rats take contact with CMs in co-culture. SNs are marked with tyrosine hydroxylase (TOH), an enzyme involved in catecholamine synthesis, whereas CMs are stained with an antibody to cardiac troponin-I (cTnI). **B.** Higher magnification of the indicated area showing close proximity between SN axons and the CM membrane. **C.** Immunofluorescence analysis of co-cultures showing synapsin1a (green) accumulation at neuronal releasing active sites, close to cardiomyocytes stained with an antibody to cTnI (red). **D.** Confocal immunofluorescence analysis on ventricular cryosections from an adult heart co-stained with antibodies to synapsin1a (green signal) and dystrophin (red signal).

FIGURE 2

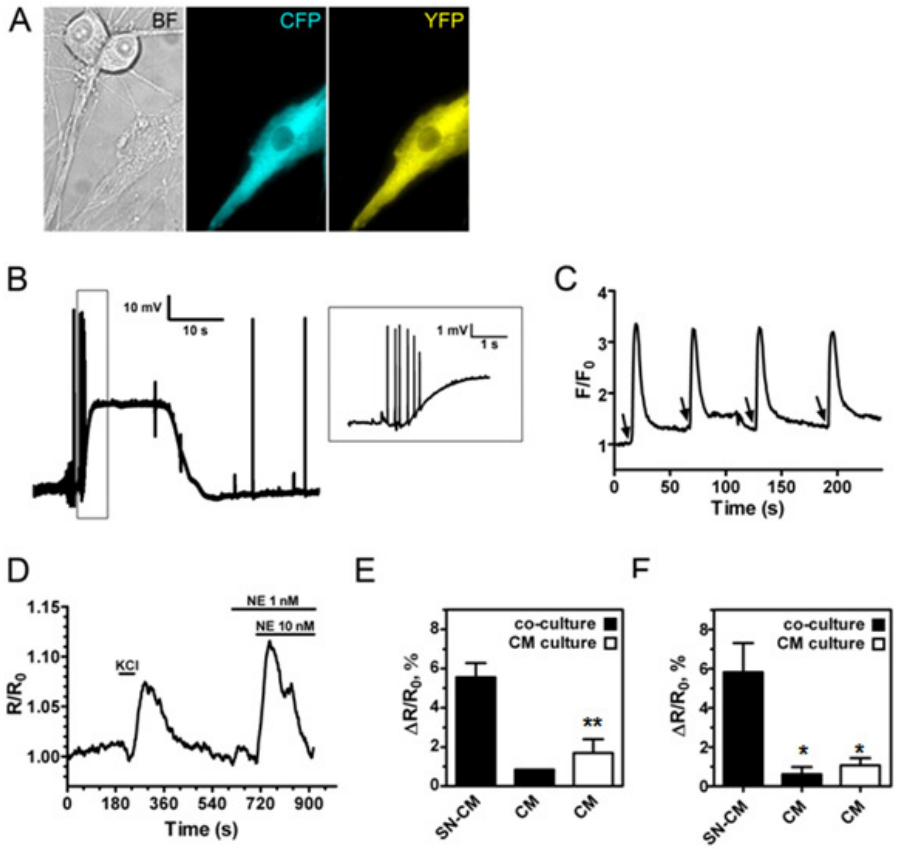

Figure 2

A. Bright field (BF) and fluorescent images of two sympathetic neurons and one target innervated neonatal cardiomyocyte expressing the FRET-based sensor EPAC1-camps. **B.** Representative membrane depolarization induced by 50 mM KCl. In the inset, depolarization-induced action potentials are shown. **C.** Depolarization-induced transients of intracellular calcium as monitored in the axon of neonatal sympathetic neurons cultured for at least 5 days in the presence of 100 ng/ml NGF and loaded with the calcium indicator Fluo4-AM. High potassium (50 mM) solution was applied for 5 s followed by washout with standard saline (5 mM KCl) every 30 s. **D.** Representative $[cAMP]_i$ increase upon KCl stimulation of SNs in one innervated CM expressed as variation in the 480/535 nm ratio upon excitation at 430 nm over the value at time t=0 (R/R_0). In the same graph, the $[cAMP]_i$ increase after addition of NE to the cell bath is also shown. **E.** Quantification of $[cAMP]_i$ increase upon KCl stimulation in innervated CM (CM-SN), non innervated cells in co-culture and myocytes cultured alone. **F.** Quantification of PKA activity as detected with the biosensor AKAR3-cyt upon KCl stimulation. *, $p < 0.05$; **, $p < 0.005$

FIGURE 3

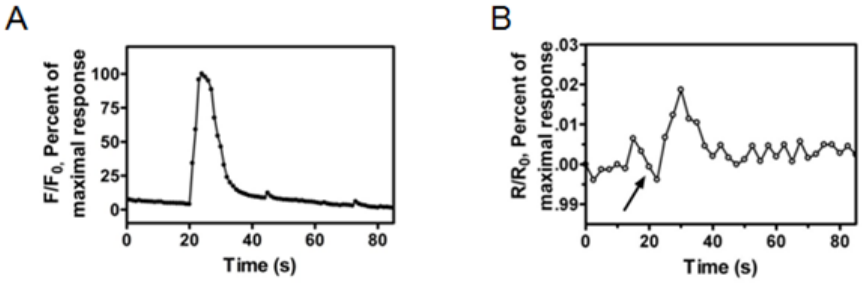

Figure 3

A. Representative trace of intracellular Ca^{2+} increase in a SN depolarized by applying a pressure of 5-10 psi for 10 s through the tip of a picospritzer pipette placed in proximity. The arrow indicate the time when pressure application was started. **B.** Representative trace of $[cAMP]_i$ increase in a CM coupled to a SN upon depolarization of the SN by applying a pressure of 5-10 psi for 10 s through the tip of a picospritzer pipette placed in proximity to the SN. The arrow indicate the time when pressure application was started.

FIGURE 4

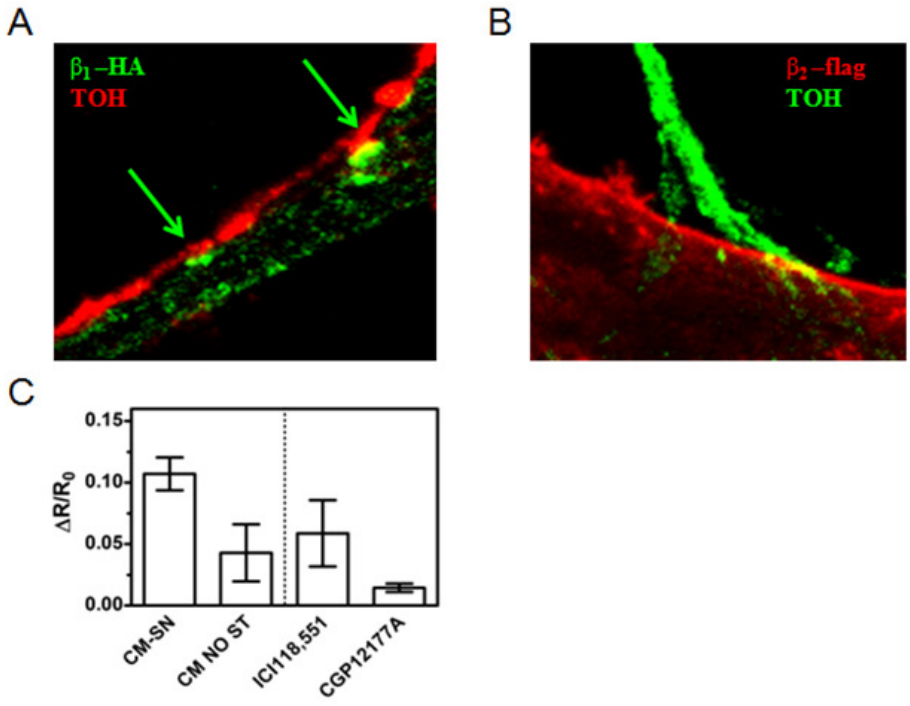

Figure 4

A. Confocal image of SN co-cultured with CM expressing a plasmid encoding for β_1-ARs fused with an HA tag. SN are stained with an anibody to tyrosine hydroxilase (red), and β_1-Ars are stained with an antibody to HA (green). The arrow indicate accumulation of the receptor under the synaptic terminal **B.** Confocal image of SN co-cultured with CM expressing a plasmid encoding for β_2-ARs fused with a flag tag. SN are stained with an anibody to tyrosine hydroxilase (green), and β_1-Ars are stained with an antibody to HA (red). The receptor are evenly distributed in the cell membrane **C.** Graph represented cAMP response in CM upon co-cultured SN stimulation in presence of either selective β_1-blocker (CGP), or selective β_2-blocker (ICI) . By blocking β_1-ARs the cAMP increase is lower than blocking β_2-ARs, suggesting that the response induced by SN is mediated mainly by β_1-ARs.

FIGURE 5

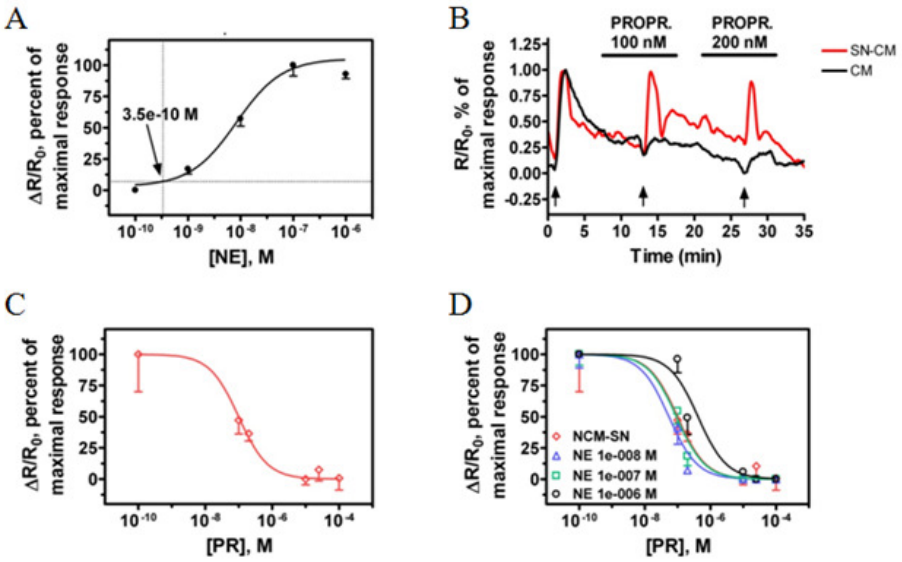

Figure 5

A. Dose/response analysis of NE as performed in CM expressing EPAC1-cAMPs. By plotting the FRET change of EPAC1-camps in CM obtained by SN stimulation in the NE dose/response curve, we obtained a value of [NE] in the order of 0.35 nM (dotted lines). This [NE] was used as control for the experiments with the antagonist propranolol (PROPR). The increase in $[cAMP]_i$ in the CMs coupled to SN was assessed in the presence of different concentrations of propranolol (**B**, representative trace in red), where arrows indicate KCl stimulation. In the presence of both 100 nM and 200 nM propranolol, an increase in $[cAMP]_i$ comparable to that without antagonist was detected. In contrast, the administration of the amount of NE that causes the same increase in cAMP to the cell bath (0.35 nM giving $\Delta R/R_0 = 2.6$ %) results in a response that is abolished by propranolol (black trace). This result indicates that the [NE] in the synaptic cleft is higher than 0.35 nM. To further investigate this aspect, the dose/response curve of $[cAMP]_i$ increase in SN-coupled CM in the presence of propranolol was built up (**C**), expressed as percent of maximal response. The comparison between the dose response curve and the EC_{50} of propranolol in presence of different concentrations of NE with that measured in presence of SN NE release (red, NCM-SN) (**D**), indicates that the response induced by SN stimulation is similar to that of 100 nM of NE. This result suggests that the concentration of NE in the synaptic cleft is about 100 nM.

REFERENCES

1. Arora, R.C., et al. (2003) *Intrinsic cardiac nervous system in tachycardia induced heart failure*. Am J Physiol Regul Integr Comp Physiol **285**, R1212-23 DOI: 10.1152/ajpregu.00131.2003.
2. Bohm M Fau - La Rosee, K., et al., *Evidence for reduction of norepinephrine uptake sites in the failing human heart.* J. Am Coll Cardiol 1995 Jan(0735-1097 (Print)).
3. Landis, S.C. (1976 Nov) *Rat sympathetic neurons and cardiac myocytes developing in microcultures: correlation of the fine structure of endings with neurotransmitter function in single neurons*. Proc Natl Acad Sci, U. S. A.
4. Conforti L Fau - Tohse, N., N. Tohse N Fau - Sperelakis, and N. Sperelakis (1991 Apr) *Influence of sympathetic innervation on the membrane electrical properties of neonatal rat cardiomyocytes in culture*. J. Dev Physiol.
5. Potter, D.D., et al. (1986) *Synaptic functions in rat sympathetic neurons in microcultures. II. Adrenergic/cholinergic dual status and plasticity*. J Neurosci **6**, 1080-98.
6. Shcherbakova, O.G., et al. (2007) *Organization of beta-adrenoceptor signaling compartments by sympathetic innervation of cardiac myocytes*. J Cell Biol **176**, 521-33 DOI: 10.1083/jcb.200604167.
7. Zaika, O., J. Zhang, and M.S. Shapiro (2011) *Functional role of M-type (KCNQ) K(+) channels in adrenergic control of cardiomyocyte contraction rate by sympathetic neurons*. J Physiol **589**, 2559-68 DOI: 10.1113/jphysiol.2010.204768.
8. Ogawa, S., et al. (1992) *Direct contact between sympathetic neurons and rat cardiac myocytes in vitro increases expression of functional calcium channels*. J Clin Invest **89**, 1085-93 DOI: 10.1172/jci115688.
9. Marvin Wj Jr Fau - Atkins, D.L., et al. (1984 Jul) *In vitro adrenergic and cholinergic innervation of the developing rat myocyte*. Circ, Res
10. Dae, M.W., et al. (1997) *Heterogeneous sympathetic innervation in German shepherd dogs with inherited ventricular arrhythmia and sudden cardiac death*. Circulation **96**, 1337-42.
11. Meredith, I.T., et al. (1991) *Evidence of a selective increase in cardiac sympathetic activity in patients with sustained ventricular arrhythmias*. N Engl J Med **325**, 618-24 DOI: 10.1056/nejm199108293250905.
12. Meredith It Fau - Eisenhofer, G., et al. (1993 Jul) *Cardiac sympathetic nervous activity in congestive heart failure. Evidence for increased neuronal norepinephrine release and preserved neuronal uptake*. Circulation, .
13. Kiuchi K Fau - Shannon, R.P., et al. (1993 Mar) *Myocardial beta-adrenergic receptor function during the development of pacing-induced heart failure*. J. Clin Invest
14. Myles, R.C., et al. (2012) *Local beta-adrenergic stimulation overcomes source-sink mismatch to generate focal arrhythmia*. Circ Res **110**, 1454-64 DOI: 10.1161/circresaha.111.262345.
15. Snider, W.D. (1994 Jun 3) *Functions of the neurotrophins during nervous system development: what the knockouts are teaching us*. Cell, .

16. Lockhart St Fau - Turrigiano, G.G., S.J. Turrigiano Gg Fau - Birren, and S.J. Birren (2008 Jun) *Nerve growth factor modulates synaptic transmission between sympathetic neurons and cardiac myocytes*. J. Neurosci
17. Ponsioen B Fau - Zhao, J., et al. (2004 Dec) *Detecting cAMP-induced Epac activation by fluorescence resonance energy transfer: Epac as a novel cAMP indicator*. Embo Rep
18. Zaglia T Fau - Milan, G., et al., *Cardiac sympathetic neurons provide trophic signal to the heart via beta2-adrenoceptor-dependent regulation of proteolysis.* Cardiovasc, Res 2013 Feb 1(1755-3245 (Electronic)).
19. Zhang J Fau - Ma, Y., et al. (2001 Dec 18) *Genetically encoded reporters of protein kinase A activity reveal impact of substrate tethering*. Proc Natl Acad Sci, U. S. A. .
20. Shcherbakova Og Fau - Hurt, C.M., et al., *Organization of beta-adrenoceptor signaling compartments by sympathetic innervation of cardiac myocytes.* J. Cell Biol 2007 Feb 12(0021-9525 (Print)).
21. Nikolaev, V.O., et al. (2006) *Cyclic AMP imaging in adult cardiac myocytes reveals far-reaching beta1-adrenergic but locally confined beta2-adrenergic receptor-mediated signaling*. Circ Res **99**, 1084-91 DOI: 10.1161/01.RES.0000250046.69918.d5.
22. Klemm M Fau - Hirst, G.D., G. Hirst Gd Fau - Campbell, and G. Campbell, *Structure of autonomic neuromuscular junctions in the sinus venosus of the toad.* J. Auton Nerv Syst 1992 Jun 15(0165-1838 (Print)).
23. Bennett Mr Fau - Gibson, W.G., J. Gibson Wg Fau - Robinson, and J. Robinson, *Probabilistic secretion of quanta: spontaneous release at active zones of varicosities, boutons, and endplates.* Biophys, J., 1995 Jul(0006-3495 (Print)).
24. Cao, J.M., et al. (2000) *Relationship between regional cardiac hyperinnervation and ventricular arrhythmia*. Circulation **101**, 1960-9.
25. Chen, L.S., et al. (2007) *New perspectives on the role of autonomic nervous system in the genesis of arrhythmias*. J Cardiovasc Electrophysiol **18**, 123-7 DOI: 10.1111/j.1540-8167.2006.00590.x.

In the first part of my PhD I started working with ChR2 and analyzed the structure/function relationship of the protein using a bioinformatic model, in combination with site directed mutagenesis and electrophysiology.

Supplemental Material can be found at:
http://www.jbc.org/content/suppl/2011/12/02/M111.326207.DC1.html

THE JOURNAL OF BIOLOGICAL CHEMISTRY VOL. 287, NO. 7, pp. 4818–4825, February 10, 2012

Bioinformatic and Mutational Analysis of Channelrhodopsin-2 Protein Cation-conducting Pathway*[S]

Received for publication, November 22, 2011 Published, JBC Papers in Press, December 2, 2011, DOI 10.1074/jbc.M111.326207

Anna Pia Plazzo[‡§1], **Nicola De Franceschi**[§¶1], **Francesca Da Broi**[‡§], **Francesco Zonta**[‖], **Maria Federica Sanasi**[‡], **Francesco Filippini**[¶], **and Marco Mongillo**[‡§2]

From the Departments of [‡]*Biomedical Sciences and* [¶]*Biology, University of Padova, viale Colombo 3, 35100 Padova, the* [‖]*Department of Physics, University of Padova, via Marzolo 8, 35100 Padova, and the* [§]*Venetian Institute of Molecular Medicine (VIMM), via Orus 2, 35129 Padova, Italy*

Background: ChR2 is a light-gated ion channel allowing fast non-invasive control of cell membrane potential.
Results: We combined bioinformatic modeling and electrophysiology to infer structure/function details on ChR2.
Conclusion: We show a complete structural model of the channel, describe the ion-conducting pathway and identify key residues involved in ionic permeability and in photoactivation.
Significance: These results expand our knowledge on the structural determinants of ChR2.

Channelrhodopsin-2 (ChR2) is a light-gated cation channel widely used as a biotechnological tool to control membrane depolarization in various cell types and tissues. Although several ChR2 variants with modified properties have been generated, the structural determinants of the protein function are largely unresolved. We used bioinformatic modeling of the ChR2 structure to identify the putative cationic pathway within the channel, which is formed by a system of inner cavities that are uniquely present in this microbial rhodopsin. Site-directed mutagenesis combined with patch clamp analysis in HeLa cells was used to determine key residues involved in ChR2 conductance and selectivity. Among them, Gln-56 is important for ion conductance, whereas Ser-63, Thr-250, and Asn-258 are previously unrecognized residues involved in ion selectivity and photocurrent kinetics. This study widens the current structural information on ChR2 and can assist in the design of new improved variants for specific biological applications.

Channelrhodopsins are light-gated ion channels that form the phototactic machinery of the unicellular alga *Chlamydomonas reinhardtii* (1). They are seven-transmembrane domains proteins and contain the light-isomerizable chromophore all-*trans*-retinal covalently bound to the protein via a protonated Schiff base.

Channelrhodopsin-2 (ChR2)[3] is a light-activated cation channel (2, 3), which can be used to control with millisecond resolution Na^+ permeability of the cell membrane. Exogenous expression of ChR2 has been exploited to achieve non-invasive control of membrane potential in neuronal cells in the intact brain (4–9) and, more recently, in cardiac cells and tissue (10, 11). A number of new channelrhodopsin variants have recently been generated with the aim to modify spectral properties of the photoprotein, ionic conductance, as well as efficiency in membrane localization and protein expression (12, 13). For instance, introduction of H134R mutation in the ChR2 sequence has yielded a variant with increased photocurrent amplitude (14), and further mutation of the Glu-123 residue to threonine led to faster off-kinetics (15). Other investigators have identified and modified those residues involved in ChR2 photocycle (15–17). Recently, the E123T/T159C double mutant that combines both large photocurrents and accelerated photocycle was generated (18).

To allow the production of new variants with characteristics suited for improved biological applications, it is essential to identify the residues involved in the basic functions of ChR2, such as the photocurrent kinetics and ionic selectivity. The identification of the determinants of ion conductance and selectivity is of great interest as it would allow the design of mutations able to optimize ChR2 properties in accordance with the application of interest and allow the widening of ChR2 application fields.

To get a deeper understanding of the ChR2 structure and of the mechanism of cation conductance, we have developed a bioinformatic model of ChR2 from *C. reinhardtii* by threading and homology modeling. This allowed us to identify two chambers that are part of the ion pathway inside the channel. The identification of putative important residues for ion conductance and selectivity was validated by patch clamp analysis of HeLa cells expressing the ChR2 mutants. A single point mutation (Q56E) of residues exposed in these two chambers allowed us to decrease conductance to Na^+, the main ChR2-permeating ion. Three variants with a single amino acid mutation displayed a different Ca^{2+}-to-Na^+ conductance ratio (S63D, T250E, and N258D) and faster off-kinetics (T250E). These results support the model and identify residues along the cation pathway, thus adding information for engineering new variants with different ion selectivity and photocurrent kinetics.

* This work was supported by funding from the European Community Seventh Framework Program FP7/2007-2013 under Grant Agreement HEALTH-F2-2009-241526, EUTrigTreat (to M. M.).
[S] This article contains supplemental Tables S1 and S2 and Figs. S1–S3.
[1] Both authors contributed equally to this work.
[2] To whom correspondence should be addressed. Tel.: 39-049827229; Fax: 39-049827250; E-mail: marco.mongillo@unipd.it.
[3] The abbreviations used are: ChR2, channelrhodopsin-2; BR, bacteriorhodopsin; AR, archaerhodopsin; HR, halorhodopsin.

EXPERIMENTAL PROCEDURES

Molecular Biology and Expression of ChR2 and Its Variants in HeLa Cells—PCR-based site directed mutagenesis was performed with oligonucleotides carrying the specific mutation using *Pfu* DNA polymerase (Stratagene, La Jolla, CA). All constructs were verified by sequencing.

HeLa cells devoid of connexins (K. Willecke, University of Bonn, Germany) (19) were used to minimize electrical noise and avoid electrical coupling between cells. Cells were grown in DMEM supplemented with 10% FBS, 2 mM glutamine, and 1% penicillin/streptomycin under a 5% CO_2 atmosphere at 37 °C. Transient transfection of cells was obtained with Lipofectamine (Invitrogen, Paisley, UK) reagent following the manufacturer's instructions. Cells were used for experiments 40–72 h after transfection, when the largest fraction of the protein reached the plasma membrane. Transfected cells were identified based on their fluorescence when imaged using a red fluorescence cube (excitation, 515 ± 35 nm; emission, 590 long pass).

To estimate protein expression, cells were fixed with 4% paraformaldehyde 48 h after transfection and imaged with an inverted confocal microscope (TCS SP5, Leica Mikrosysteme Vertrieb GmbH) equipped with oil immersion objectives (Leica 63×, 1.4 NA). Cells transfected with ChR2(H134R)-mCherry and respective mutants were excited by the 561-mm laser line, and emission was collected between 570 and 660 nm. For intracellular Ca^{2+} imaging, Fluo-4 (1 μM, Molecular Probes, Invitrogen) was loaded at 37 °C for 30 min. Cells were then washed and transferred into an extracellular solution consisting of 80 mM Ca^{2+}, 5 mM Na^+, 3 mM KCl, 135 mM *N*-methyl-D-glucamine, 10 mM Hepes, 20 mM glucose, adjusted at pH = 7.4. Fluo-4 and ChR2 were excited with 100-ms pulses of 490 ± 20 nm, and the emitted light was detected with a CCD camera at 510 ± 20 nm.

Electrophysiology—Whole cell patch clamp experiments were performed at room temperature (~23 °C) on single cells visualized with an inverted microscope (Olympus IX50, Tokyo, Japan). Photocurrents were activated with a 500-ms pulse of 470-nm light and recorded using an EPC-7 amplifier (HEKA Electronik, Lambrecht, Germany) and the Axon Instruments pClamp10 software. Data were sampled at 10 kHz.

Patch pipettes were prepared by pulling borosilicate glass capillaries (1.5-mm outer diameter and 1.16-mm inner diameter, Harvard Apparatus Ltd.) using a micropipette puller (Narishige). Pipette resistance was 2.3–3.5 megaohms when filled with intracellular solution.

Extracellular solutions contained (in mM): 145 NaCl, 3 KCl, 5 *N*-methyl-D-glucamine, 10 Hepes, 20 Glucose; pH was adjusted to 7.35 with HCl (solution 1). Ca^{2+} photocurrents were recorded in (in mM): 3 KCl, 135 *N*-methyl-D-glucamine, 10 $CaCl_2$, 10 Hepes, 20 glucose; pH was adjusted to 7.35 with HCl (solution 2). Intracellular solution was (in mM): 120 CsCl, 10 triethanolamine-Cl, 10 Hepes, 10 EGTA, 4 MgATP, 0.1 NaGTP; pH was adjusted to 7.2 with CsOH.

Light stimulation was provided by a 100-watt mercury lamp equipped with a mechanical shutter (Uniblitz, Vincent Associates, Rochester, NY) with the light filtered through a 480 ± 10-nm band-pass filter (Chroma, Bellows Falls, VT) and reflected off a mirror to the specimen through a 40×, 1.4 NA oil immersion objective (Olympus). This resulted in light power at the sample plan of 0.45 milliwatt/mm^2. ChR2 activation spectra were acquired using a monochromator (Polychrome IV, Till Photonics GmbH) triggered via the D/A port of the Digidata interface driven by pClamp 10 (Axon Instruments).

Structure Modeling—ChR2 1–315 models were obtained using the Protein Homology/analogY Recognition Engine (Phyre) Server (20) and the Swiss-Model server (21). The models are based on the following templates: 1m0kA (model 1, 7.0×10^{-26}), 1xioA (model 2, 6.2×10^{-27}), 1h2sA (model 3, 1.3×10^{-26}), and 1h2sA (model 4, 2.0×10^{-44}). Retinal was added in the final models by juxtaposition. The Protein3Dfit server was used for structural superposition (22), and the PyMOL viewer was used for visualization (Schrödinger LLC, Portland, OR) (23). The models underwent energy minimization and a short molecular dynamics simulation (100 ps) with constrained α-carbon position to allow the side chain to relax. Both energy minimization and molecular dynamics studies were performed using the Amber94 force field (24) and the Gromacs molecular dynamics package (25). Energy minimization was performed *in vacuo*, whereas for molecular dynamics, we solvated the proteins using an explicit solvent model (TIP3) and an ion concentration of 0.15 M NaCl. The system was then simulated under periodic boundary conditions at 300 K and 1 atm using the Berendsen thermostat and barostat (26). To investigate the effect of the R120A mutation, we performed unrestrained molecular dynamics for model 2 and for the same model in which Arg-120 was mutated into an alanine. The dynamics of the two systems were followed for 1 ns to let the side chains relax, without the restraint on the α-carbon positions. The simulation conditions were the same as the equilibration described above.

RESULTS

ChR2 Bioinformatic Models—To investigate the structural features of ChR2, we developed four models of the protein by both threading and homology modeling of the fragment 1–315 of ChR2(H134R) from *C. reinhardtii*. ChR2 models 1, 2, and 3 were obtained by the Phyre Server (20), and model 4 was obtained by the Swiss-Model server (21). In all models, only the central part of the sequence is represented (residues 52–273 in models 1, 2, and 3 and residues 56–263 in model 4), resulting in the classic rhodopsin fold based on seven-transmembrane antiparallel α helices, predicted to have an extracellular N terminus and an intracellular C terminus (supplemental Fig. S1, A and B). Residues composing the transmembrane helices are indicated in supplemental Table S1.

The loops connecting such helices are short (≤10 amino acids) except for the α2-α3 loop, which in most models is up to 16 residues long. This extended loop, which includes a short helix in model 2, is located on the extracellular side of the membrane, on the same side as the N-terminal extracellular region (the first 50 residues at the N-terminal are not modeled). The α2-α3 loop and the N terminus are rich in hydrophobic residues. In HR, a similar structure is present that has been proposed to function as a regulator of the ion flux (6). Although

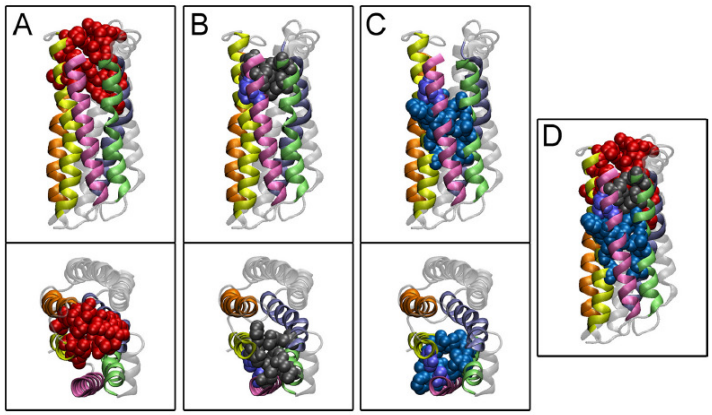

FIGURE 1. **Inner chamber system in ChR2 according to molecular modeling.** Spatially conserved chambers in ChR2 bioinformatic model 2 are shown. *A–C*, chamber A (*A*), chamber B (*B*), and chamber C (*C*) with their side and top view. Helices surrounding the chambers are colored in *mauve* (helix 1), *green* (helix 2), *blue* (helix 3), *orange* (helix 6), and *yellow* (helix 7). In *D*, superposition of all chambers is shown.

there is general agreement on the residues being part of the last five TM helices of ChR2, sequence homology of helices 1 and 2 with other rhodopsins is low. We took into account structural information from homology and threading modeling to obtain a structure-based alignment of these two helices (supplemental Fig. S2).

Sequence alignment and structure superimposition with HR, BR, and a third light-driven proton pump with known structure, archaerhodopsin (AR) (27, 28) (Protein Data Bank accession numbers: 3a7k, 2zzl, and 2ei4, respectively), were used to investigate the structural features of ChR2. Superposition of the four ChR2 models with HR, BR, and AR allowed us to identify a structure corresponding to the retinal binding pocket previously identified in the other rhodopsins. In our models, Lys-257 results in the correct position to be covalently bound to the retinal forming a Schiff base, which is in line with current evidence. The aromatic residues surrounding the retinal are Trp-124, Phe-178, Tyr-184, Trp-223, Phe-226, and Phe-230 (supplemental Table S2), showing a high degree of homology with the corresponding residues in HR (29). The proton donor and acceptors for the retinal Schiff base were reported to be Arg-134, Glu-123, and Asp-253, respectively (16). Accordingly, in our model, Arg-134 and Glu-123 are located on opposite sides with respect to the retinal. The first is located toward the intracellular part, about 11.6 Å from the Schiff base, whereas the second is located toward the protein extracellular side, at about 4.1 Å from the Schiff base. The other residues described to be involved in the ChR2 photocycle are Cys-128 and Asp-156 (16, 30–32); in our model, they point toward the retinal pocket with their sulfur and oxygen atoms at a relative distance of 2.6 Å, compatible with formation of a hydrogen bond.

Inner Chamber System and Ion Selectivity Filter in ChR2—Internal water-filled cavities have been described in BR and microbial rhodopsins (33), and a system of inner chambers determines the ion pathway in ion-conducting rhodopsin (29). In our ChR2 models, we identified a system of inner chambers in the extracellular half of the protein. Three spatially conserved chambers, hereafter named chambers A, B, and C, were present in the ChR2 models (Fig. 1). Among these, only chamber A (located toward the extracellular side) is also present in HR, AR, and BR. By contrast, chambers B and C seem to be a specific feature of ChR2 because only partial superposition with HR, AR, and BR chambers is found (not shown). The inner surface of chambers B and C is formed by both polar/charged residues, whose spatial position is well conserved in the different simulations, and hydrophobic residues whose identity and position are less well defined. This accounts for the different shape and size of the chambers among the models. A list of the residues that form the surface of chambers B and C in the corresponding models can be found in Table 1. The structural features of the inner chambers and their position within ChR2 suggest that they are likely to form the cationic pathway. Our model is consistent with a role of the negatively charged and polar side chains of the two consecutive chambers B and C in coordinating and progressively dehydrating the ion while it proceeds along the channel cavity. Therefore, we designed a set of point mutations in chambers B and C (Fig. 2) to change the geometry and the charge distribution of the chambers. In the first set of mutants, we aimed at increasing the net negative charge of the residues facing the inner chambers to allow dehydration of ions with higher charge density (small divalent cations, *i.e.* Ca^{2+}) than Na^{+}. Therefore, selected residues were mutated to either Asp or Glu to change as little as possible the bulk of the side chain. In the case of the mutant A59S, we sought to modify the geometry of the coordination site, adding a further polar contact.

Functional Characterization of ChR2 Mutants—ChR2 mutants tagged with the fluorescent mCherry protein fused at the C terminus were expressed in HeLa cells and tested by whole cell voltage clamp. Photocurrents were evoked by a 500-ms pulse of blue light (480 ± 10 nm, 0.45 milliwatt/mm^2) and measured at different membrane potentials (20-mV steps

TABLE 2

Kinetic properties of ChR2(H134R)-mCherry and respective mutant variants. Opening rates (τ_{ON}), closing rates (τ_{OFF}), and desensitization rates (τ_{DES}) were estimated from photocurrents of at least six cells. Values represent means ± S.E. * = $p < 0.01$, unpaired *t* test. I_{max} is the largest peak current, and $I_{plateau}$ is the current at the steady state level

	$I_{Plateau}/I_{Max}$	τ_{ON}	τ_{OFF}	τ_{DES}
		ms	*ms*	*ms*
WT	75.8 ± 4.8	2.17 ± 0.26	14.94 ± 1.24	9.18 ± 0.64
Q56E	71.1 ± 4.3	3.78 ± 0.61*	14.56 ± 0.46	11.75 ± 0.06
A59S	71.3 ± 3.3	1.56 ± 0.14	12.76 ± 1.08	8.26 ± 1.45
S63D	83.3 ± 2.2*	1.64 ± 0.10	17.26 ± 0.90	15.27 ± 1.06*
T250D	71.1 ± 3.2	2.44 ± 0.25	12.72 ± 0.48	9.89 ± 0.97
T250E	68.4 ± 4.0*	2.42 ± 0.18	8.21 ± 0.70*	11.83 ± 1.85
N258D	82.7 ± 2.4*	2.29 ± 0.16	27.42 ± 0.96*	25.83 ± 3.07*

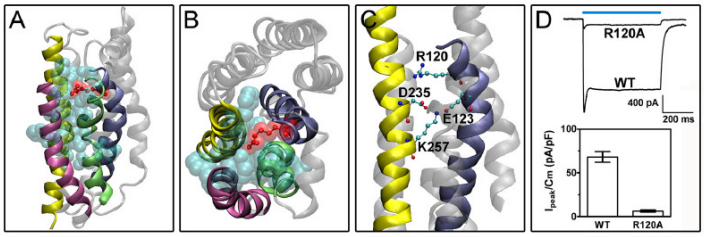

FIGURE 4. **Role of ARS-120 in the counterion system.** *A* and *B*, side chain of residue Arg-120 (in *red*) obstructs cation pathway (represented by chambers B and C, in *cyan*), as shown for ChR2 model 2 after a 1-ns molecular dynamics simulation (*A*, side view; *B*, top view). *C*, enlargement of the Schiff base region, with the key residues forming the hydrogen bond network. Arg-120 is found in a position in between the counterions Glu-123 and Asp-253, at a relative distance of 7.4 and 4.6 Å, respectively. *D*, R120A mutation caused a 10-fold reduction in photocurrent amplitude. In the graphs, currents at −120 mV in solution 1 are shown, $n = 10$). *pF*, picofarads. *Error bars* in indicate S.D.

Role of Counterion System in ChR2 Photoactivation—As suggested by sequence similarity and functional data, the activation mechanism of ChR2 is similar to other microbial rhodopsins, and our bioinformatic model is in agreement with this concept. In BR, the proton transfer occurs in an extended hydrogen-bonded complex containing the two negatively charged Asp-85 and Asp-212, two positively charged groups, Lys-216 (the Schiff base) and Arg-82, and coordinated water (35). In our ChR2 models, the corresponding residues are predicted to be Glu-123, Asp-253, Lys-257 (the Schiff base), and Arg-120, respectively.

We used molecular dynamics simulations to include water in our model and explore equilibrium fluctuations of the side chains. Quite intriguingly, after 1 ns, the side chain of Arg-120 faces chamber B and obstructs the cation pathway (Fig. 4, *A* and *B*) as corresponding basic residues in BR and HR do (33). Arg-120 is found in a position in between the counterions Glu-123 and Asp-253, at a relative distance of 7.4 and 4.6 Å, respectively (Fig. 4*C*). This is consistent with the structure of BR, in which these 4 residues and a centrally coordinated water molecule form a quadrupole (36).

To test whether Arg-120 is involved in the mechanism of photoactivation, we substituted the arginine with a non-protonable alanine (R120A). Energy minimization of the ChR2 R120A model demonstrated that this mutation does not alter the structure of the helices and protein stability and that its position did not change upon molecular dynamics simulation. Photocurrent of R120A mutant was compared with that of the wild type ChR2 in a subset of cells with comparable expression levels at the plasma membrane. We found that R120A mutation caused a 10-fold reduction in photocurrent amplitude (Fig. 4*D*).

DISCUSSION

In this study, we used a combination of bioinformatic modeling, molecular dynamics simulations, and site-directed mutagenesis to gain information on structure-function relationship in ChR2. Bioinformatic structure prediction and structural superposition of ChR2 with BR, AR, and HR, other microbial rhodopsins with ion conductance, allowed us to identify the putative ion pathway within the channel. In ChR2, this is formed by a series of three consecutive chambers made by residues belonging to helices 1–4 and 7. Among these, only chamber A (located toward the extracellular side) is also present in HR, AR, and BR. By contrast, chambers B and C are a specific feature of ChR2. Internal water-filled cavities have been described in BR and microbial rhodopsins (33), and a system of inner chambers determines the ion pathway in ion-conducting rhodopsin (29).

Mutagenesis of residues predicted to be exposed in chambers B and C caused alterations in conductance to Na^+ (Q56E) or relative Ca^{2+} or Na^+ conductance (S63D, T250E, and N258D), supporting that these residues participate in the pore formation. It has been reported that only dehydrated cations can permeate the "selective filter" of ChR2 (3). Our structural modeling of the ion conduction pathway is consistent with a role of the negatively charged and polar side chains of the two consecutive chambers B and C in coordinating and progressively dehydrating the ion while it proceeds along the channel cavities. The experimental evidence suggests that adding further polar residues to chamber B has a negative or no effect on ion current. On the contrary, increasing the net negative charge exposed in chamber C results in a higher Ca^{2+}/Na^+ current ratio. Given that Ca^{2+} has a higher charge density and bigger hydration

shell than Na^+, this may indicate that a limiting step in the dehydration process occurs mostly in chamber C.

To our knowledge, most of the ChR2 mutations have been engineered so far on the basis of sequence homology to BR, whose crystal structure is known in detail, and have targeted regions close to the retinal binding pocket (helix 2 and 3). This has generated a number of mutants with increased photocurrent and altered kinetics. Among these, only L132C mutation affected the relative permeability to Ca^{2+} and Na^+ (37). Our analysis explores a new region of the protein, suggesting new determinants for ion selectivity and permeability (Ser-63 and Asn-258).

In previous models of ChR2, several glutamic acid residues in helix B (Glu-82, Glu-83, Glu-90, Glu-97, and Glu-101) were predicted (i) to be part of the water-containing cavity allowing ions to cross the channel and (ii) to point toward the outer part of the ring formed by the seven-transmembrane helices (38), suggesting that the functional ChR2 may work as a trimer. However, no evidence in favor of the trimeric unit was provided in other studies (39, 40).

In addition, ChR2 was recently shown to form dimers rather than trimers, and the arrangement of the monomers does not seem to support this latter model (41). However, these negatively charged residues represent a striking feature of helix 2 in our alignment as well (supplemental Fig. S2), and at least some of those were shown to affect the photocurrent (42, 43).

In our models, despite a linear arrangement of their Cα, residues Glu-82, Glu-83, and Glu-90 are located on the surface of the protein, pointing toward the outside of the monomer, whereas Glu-101 points to the interior of the ring of helices. The exact position of the side chain of Glu-97 is uncertain as in different models, it bends over either the ring of helices or the external surface. One possible explanation might be that helix 2 can exist in different degrees of rotation, which could represent different conformational states of the protein during the photocycle.

The mechanism of functioning of ChR2 is similar to other microbial rhodopsins. ChR2 has been proposed to function as a proton pump, with a proton "leak" suggested as a basis of its ion channel behavior (44).

As mutation R120A almost entirely abolished the photocurrent, and given the position of this residue between the putative counterions Glu-123 and Asp-253, it can be speculated that electrostatic interactions of the charged side chain of Arg-120 take part in the mechanism of photoactivation. This would be in line with the general proton-pumping mechanism of rhodopsins, as recently described using BR as a model (33).

In BR, deprotonation of the Schiff base Lys-216 (Lys-257 in ChR2) upon photon absorption breaks its interaction with the counterions Asp-85 and Asp-212 (Glu-123 and Asp-253 in ChR2). This event breaks the salt bridge between Asp-85 and Arg-82 (Arg-120 in ChR2), and this latter in turn moves toward Glu-194/Glu-204 (Glu-235/Ser-245 in ChR2), and by this mechanism, a proton is released to the bulk.

The homology of the structural features of BR and ChR2 in the Schiff base region of the retinal binding site further supports the concept of a similar molecular basis of the photoactivation mechanism. Therefore, we propose that the proton-pumping mechanism in ChR2 proceeds by displacement of the side chain of Arg-120 following protonation of the Schiff base counterion.

In BR, electrostatic interaction between the Schiff base and the surrounding residues in the binding pocket affects the retinal absorption spectrum. It is thus tempting to speculate that mutagenesis in the residues surrounding the Schiff base region may result in spectrally shifted variants.

In conclusion, we show a complete structural model of ChR2, describe the ion-conducting pathway, and identify novel key residues involved in ionic permeability and in the photoactivation mechanism. These results expand our current knowledge on the structural determinants of ChR2 function and direct further biotechnological efforts to generate new variants with specific biophysical properties (*i.e.* higher Ca^{2+} conductance, higher Na^+ specificity, faster/slower kinetics). Notably, most of our mutants were obtained by targeting previously unrecognized regions regulating ChR2 function. Possible combination with existing variants may therefore be used to tune ChR2 function to specific applications.

Acknowledgments—We thank Prof. Peter Hegemann (Humboldt University of Berlin, Germany) and Prof. Tullio Pozzan (University of Padova, Italy) for helpful discussion and Prof. Karl Deisseroth (Stanford University, Stanford, CA) for the ChR2(H134R)-mCherry construct. We are indebted to Dr. Andrea Lelli for the technical help.

REFERENCES

1. Foster, K. W., Saranak, J., Patel, N., Zarilli, G., Okabe, M., Kline, T., and Nakanishi, K. (1984) A rhodopsin is the functional photoreceptor for phototaxis in the unicellular eukaryote *Chlamydomonas*. *Nature* **311,** 756–759
2. Nagel, G., Ollig, D., Fuhrmann, M., Kateriya, S., Musti, A. M., Bamberg, E., and Hegemann, P. (2002) Channelrhodopsin-1: a light-gated proton channel in green algae. *Science* **296,** 2395–2398
3. Nagel, G., Szellas, T., Huhn, W., Kateriya, S., Adeishvili, N., Berthold, P., Ollig, D., Hegemann, P., and Bamberg, E. (2003) Channelrhodopsin-2, a directly light-gated cation-selective membrane channel. *Proc. Natl. Acad. Sci. U.S.A.* **100,** 13940–13945
4. Boyden, E. S., Zhang, F., Bamberg, E., Nagel, G., and Deisseroth, K. (2005) Millisecond-timescale, genetically targeted optical control of neural activity. *Nat. Neurosci.* **8,** 1263–1268
5. Zhang, F., Wang, L. P., Brauner, M., Liewald, J. F., Kay, K., Watzke, N., Wood, P. G., Bamberg, E., Nagel, G., Gottschalk, A., and Deisseroth, K. (2007) Multimodal fast optical interrogation of neural circuitry. *Nature* **446,** 633–639
6. Arenkiel, B. R., Peca, J., Davison, I. G., Feliciano, C., Deisseroth, K., Augustine, G. J., Ehlers, M. D., and Feng, G. (2007) *In vivo* light-induced activation of neural circuitry in transgenic mice expressing channelrhodopsin-2. *Neuron* **54,** 205–218
7. Zhang, F., Wang, L. P., Boyden, E. S., and Deisseroth, K. (2006) Channelrhodopsin-2 and optical control of excitable cells. *Nat. Methods* **3,** 785–792
8. Ishizuka, T., Kakuda, M., Araki, R., and Yawo, H. (2006) Kinetic evaluation of photosensitivity in genetically engineered neurons expressing green algae light-gated channels. *Neurosci. Res.* **54,** 85–94
9. Li, X., Gutierrez, D. V., Hanson, M. G., Han, J., Mark, M. D., Chiel, H., Hegemann, P., Landmesser, L. T., and Herlitze, S. (2005) Fast noninvasive activation and inhibition of neural and network activity by vertebrate rhodopsin and green algae channelrhodopsin. *Proc. Natl. Acad. Sci. U.S.A.* **102,** 17816–17821
10. Bruegmann, T., Malan, D., Hesse, M., Beiert, T., Fuegemann, C. J., Fleischmann, B. K., and Sasse, P. (2010) Optogenetic control of heart muscle *in vitro* and *in vivo*. *Nat. Methods* **7,** 897–900

11. Hofmann, B., Maybeck, V., Eick, S., Meffert, S., Ingebrandt, S., Wood, P., Bamberg, E., and Offenhäusser, A. (2010) Light-induced stimulation and delay of cardiac activity. *Lab Chip* **10,** 2588–2596
12. Hegemann, P., and Möglich, A. (2011) Channelrhodopsin engineering and exploration of new optogenetic tools. *Nat. Methods* **8,** 39–42
13. Deisseroth, K. (2011) Optogenetics. *Nat. Methods* **8,** 26–29
14. Nagel, G., Brauner, M., Liewald, J. F., Adeishvili, N., Bamberg, E., and Gottschalk, A. (2005) Light activation of channelrhodopsin-2 in excitable cells of *Caenorhabditis elegans* triggers rapid behavioral responses. *Curr. Biol.* **15,** 2279–2284
15. Gunaydin, L. A., Yizhar, O., Berndt, A., Sohal, V. S., Deisseroth, K., and Hegemann, P. (2010) Ultrafast optogenetic control. *Nat. Neurosci.* **13,** 387–392
16. Berndt, A., Yizhar, O., Gunaydin, L. A., Hegemann, P., and Deisseroth, K. (2009) Bi-stable neural state switches. *Nat. Neurosci.* **12,** 229–234
17. Stehfest, K., Ritter, E., Berndt, A., Bartl, F., and Hegemann, P. (2010) The branched photocycle of the slow-cycling channelrhodopsin-2 mutant C128T. *J. Mol. Biol.* **398,** 690–702
18. Berndt, A., Schoenenberger, P., Mattis, J., Tye, K. M., Deisseroth, K., Hegemann, P., and Oertner, T. G. (2011) High-efficiency channelrhodopsins for fast neuronal stimulation at low light levels. *Proc. Natl. Acad. Sci. U.S.A.* **108,** 7595–7600
19. Beltramello, M., Bicego, M., Piazza, V., Ciubotaru, C. D., Mammano, F., and D'Andrea, P. (2003) Permeability and gating properties of human connexins 26 and 30 expressed in HeLa cells. *Biochem. Biophys. Res. Commun.* **305,** 1024–1033
20. Kelley, L. A., and Sternberg, M. J. (2009) Protein structure prediction on the web: a case study using the Phyre server. *Nat. Protoc.* **4,** 363–371
21. Arnold, K., Bordoli, L., Kopp, J., and Schwede, T. (2006) The SWISS-MODEL workspace: a web-based environment for protein structure homology modeling. *Bioinformatics* **22,** 195–201
22. Lessel, U., and Schomburg, D. (1994) Similarities between protein three-dimensional structures. *Protein Eng.* **7,** 1175–1187
23. Lill, M. A., and Danielson, M. L. (2011) Computer-aided drug design platform using PyMOL. *J. Comput. Aided Mol. Des.* **25,** 13–19
24. Cornell, W. D., Cieplak, P., Bayly, C. I., Gould, I. R., Merz, K. M., Ferguson, D. M., Spellmeyer, D. C., Fox, T., Caldwell, J. W., and Kollman, P. A. (1995) A second generation force field for the simulation of proteins, nucleic acids, and organic molecules. *J. Am. Chem. Soc.* **117,** 5179–5197
25. Hess, B., Kutzner, C., van der Spoel, D., and Lindahl, E. (2008) Gromacs 4: algorithms for highly efficient, load-balanced, and scalable molecular simulation. *J. Chem. Theory Comput.* **4,** 435–447
26. Berendsen, H. J., Postma, J. P., van Gunsteren, W. F., DiNola, A., and Haak, J. R. (1984) Molecular dynamics with coupling to an external bath. *J. Chem. Phys.* **81,** 3684–3690
27. Enami, N., Yoshimura, K., Murakami, M., Okumura, H., Ihara, K., and Kouyama, T. (2006) Crystal structures of archaerhodopsin-1 and -2: common structural motif in archaeal light-driven proton pumps. *J. Mol. Biol.* **358,** 675–685
28. Yoshimura, K., and Kouyama, T. (2008) Structural role of bacterioruberin in the trimeric structure of archaerhodopsin-2. *J. Mol. Biol.* **375,** 1267–1281
29. Kouyama, T., Kanada, S., Takeguchi, Y., Narusawa, A., Murakami, M., and Ihara, K. (2010) Crystal structure of the light-driven chloride pump halorhodopsin from *Natronomonas pharaonis*. *J. Mol. Biol.* **396,** 564–579
30. Nack, M., Radu, I., Gossing, M., Bamann, C., Bamberg, E., von Mollard, G. F., and Heberle, J. (2010) The DC gate in channelrhodopsin-2: crucial hydrogen bonding interaction between Cys-128 and Asp-156. *Photochem. Photobiol. Sci.* **9,** 194–198
31. Radu, I., Bamann, C., Nack, M., Nagel, G., Bamberg, E., and Heberle, J. (2009) Conformational changes of channelrhodopsin-2. *J. Am. Chem. Soc.* **131,** 7313–7319
32. Bamann, C., Gueta, R., Kleinlogel, S., Nagel, G., and Bamberg, E. (2010) Structural guidance of the photocycle of channelrhodopsin-2 by an interhelical hydrogen bond. *Biochemistry* **49,** 267–278
33. Wolf, S., Freier, E., Potschies, M., Hofmann, E., and Gerwert, K. (2010) Directional proton transfer in membrane proteins achieved through protonated protein-bound water molecules: a proton diode. *Angew Chem. Int. Ed Engl.* **49,** 6889–6893
34. Tsunoda, S. P., and Hegemann, P. (2009) Glu-87 of channelrhodopsin-1 causes pH-dependent color tuning and fast photocurrent inactivation. *Photochem. Photobiol.* **85,** 564–569
35. Brown, L. S., Váró, G., Hatanaka, M., Sasaki, J., Kandori, H., Maeda, A., Friedman, N., Sheves, M., Nedleman, R., and Lanyi, J. K. (1995) The complex extracellular domain regulates the deprotonation and reprotonation of the retinal Schiff base during the bacteriorhodopsin photocycle. *Biochemistry* **34,** 12903–12911
36. Dér, A., Száraz, S., Tóth-Boconádi, R., Tokaji, Z., Keszthelyi, L., and Stoeckenius, W. (1991) Alternative translocation of protons and halide ions by bacteriorhodopsin. *Proc. Natl. Acad. Sci. U.S.A.* **88,** 4751–4755
37. Kleinlogel, S., Feldbauer, K., Dempski, R. E., Fotis, H., Wood, P. G., Bamann, C., and Bamberg, E. (2011) Ultra light-sensitive and fast neuronal activation with the Ca^{2+}-permeable channelrhodopsin CatCh. *Nat. Neurosci.* **14,** 513–518
38. Hegemann, P., and Tsunoda, S. (2007) Light tools for neuroscience: channelrhodopsin and light-activated enzymes. *Cell Sci. Rev.* **3,** 108–123
39. Hegemann, P., Ehlenbeck, S., and Gradmann, D. (2005) Multiple photocycles of channelrhodopsin. *Biophys. J.* **89,** 3911–3918
40. Petreanu, L., Huber, D., Sobczyk, A., and Svoboda, K. (2007) Channelrhodopsin-2-assisted circuit mapping of long-range callosal projections. *Nat. Neurosci.* **10,** 663–668
41. Müller, M., Bamann, C., Bamberg, E., and Kühlbrandt, W. (2011) Projection structure of channelrhodopsin-2 at 6 Å resolution by electron crystallography. *J. Mol. Biol.* **414,** 86–95
42. Ruffert, K., Himmel, B., Lall, D., Bamann, C., Bamberg, E., Betz, H., and Eulenburg, V. (2011) Glutamate residue 90 in the predicted transmembrane domain 2 is crucial for cation flux through channelrhodopsin 2. *Biochem. Biophys. Res. Commun.* **410,** 737–743
43. Sugiyama, Y., Wang, H., Hikima, T., Sato, M., Kuroda, J., Takahashi, T., Ishizuka, T., and Yawo, H. (2009) Photocurrent attenuation by a single polar-to-nonpolar point mutation of channelrhodopsin-2. *Photochem. Photobiol. Sci.* **8,** 328–336
44. Feldbauer, K., Zimmermann, D., Pintschovius, V., Spitz, J., Bamann, C., and Bamberg, E. (2009) Channelrhodopsin-2 is a leaky proton pump. *Proc. Natl. Acad. Sci. U.S.A.* **106,** 12317–12322

Optogenetic control of sympathetic neurons activity *in vitro* and *in vivo*

ChR2 photostimulation modulates activation of neuronally differentiated chromaffin cells

The aim of this part of the project is to develop an optogenetic approach to control sympathetic neuron activity with high temporal resolution and non invasively, by using ChR2. ChR- microbial proteins are light-gated channel and they were extensively used to control the activity of excitable cells [4, 5, 70, 80]. Among these light-controlled protein, ChR2 is a plasma-membrane localized protein that becomes permeable to cations (mostly Na^+) upon light stimulation at 470 nm [68]. This tool has been used also to modulate neuronal activity *in vivo*, indeed photostimulation of ChR2 trigger a depolarization sufficient to induce action potential in neuronal cells [5, 70].

To test in vitro the feasibility of such approach, we used co-cultures between neuronally differentiated chromaffin (PC12) cells and neonatal cardiomyocytes (**FIG 1A**).

PC12 cells are pheochromocytoma cell line that acquires a neuronal phenotype in presence of NGF and low concentration of serum [81], and they are able to secrete acetylcholine and NE upon depolarization-induced intracellular Ca^{2+} increase [81, 82]. PC12 cells were transiently transfected with a plasmid encoding the H134R variant of ChR2, a variant engineered to maximize current amplitude in response to light-induced depolarization [83].

To assess whether ChR2 induced a depolarization sufficient to stimulate Ca^{2+} influx in the PC12 cells, we used fluorescence Ca2+ imaging with FURA2-AM (Molecular Probes, invitrogen U.S.A). Differentiated PC12 were loaded with Fura2-AM and placed on the stage of a fluorescence microscope. Photostimulation with 200 ms pulse trains, at 460 nm caused a rapid intracellular Ca^{2+} increase ($\Delta R = 40\% \pm 3\%$) in ChR-positive cells with no effect on intracellular Ca2+ in cells not expressing ChR2 (**FIG. 1B**).

To verify whether optogenetic modulation of neuronal-differentiated PC12 cells can modulate cardiomyocyte activity, we test whether stimulate of ChR2-positive PC12 cells can modulate cardiomyocyte beating rate.

We loaded PC12/cardiomyocytes co-cultures with the intracellular Ca^{2+} indicator FURA2-AM. Neonatal cardiomyocytes contract spontaneously and display spontaneous

intracellular Ca^{2+} oscillation and respond to NE activation of β-ARs [84], with an increase of the spontaneous beating rate.

In ChR2-expressing PC12 coupled to a cardiomyocyte (**FIG. 2A)** the frequency of spontaneous Ca^{2+} transients increased significantly. This suggests that photostimulation of ChR2 induces a depolarization sufficient to trigger NE release, that interacts with the β-ARs localized in the plasmamembrane of the cardiomyocyte (**FIG 2B**).

These data suggest that the ChR-mediated control of sympathetic neurons is a feasible method to modulate the contraction frequency of cardiac cells, and could be also applied to modulate heart beating rate in living mice.

ChR2 photostimulation of SNS increase heart beating rate *in vivo*

SN depolarization lead to NE release from sympathetic nerve endings activated β-ARs leading to increase in the heart beating rate. Here, we provided a novel approach to optically depolarize neuronal-like cells inducing increase in the cardiomyocytes beating rate *in vitro*.

We used optogenetics with ChR2 to develop an experimental model for non-invasive control of cardiac sympathetic neurons. Transgenic mice expressing ChR2 in the sympathetic ganglia neurons were obtained by breeding double floxed-ChR2-mTomato mice (Jackson Lab) with a strain expressing Cre-recombinase driven by the adrenergic neuron specific tyrosine hydroxilase (TOH) promoter. The offsprings were genotyped and mice with expression of both alleles were analyzed by fluorescence microscopy. Successful recombination of the floxed ChR2 gene was demonstrated by expression of mTomato fluorescence in the superior cervical ganglia neurons (**FIG. 3A**). Superior cervical ganglia were harvested and fixed in PFA (4%), and cryo-sections were obtained in frozed, OCT cast samples. Fluorescence microscopy analysis showed that ChR2 is well expressed in the superior cervical ganglia and it is localized correctly in the plasmamembrane of the cells (**FIG. 3B**).

Function of ChR2 was determined using optical stimulation of the cervical sympathetic chain neurons and in the stellate ganglia, by delivering fast (10ms) light pulses (470nm) with a fiber optic during continuos ECG monitoring.

Mouse was anesthetized with a combination of tiletamine/zolazepam and xylazine, ventilated to allow surgical access of the deeper plans of the neck and the thorax. The mouse was connected to an ECG apparatus (**FIG. 4**). Fiber optics of different size (Thorlabs, 200µm to 1 mm diameters) were positioned at different points in the cervical sympathetic chain and both stimulation of the superior cervical ganglia and stellate ganglia, containing most cell bodies of the postganglionic sympathetic neurons projecting to the heart.

Stimulation of the left stellate ganglia with bursts of 10ms long pulses at 30Hz rate, we lead to an immediate increase in HR which averaged 40% in 10 different trials ($\Delta(HR_{basal}/HR_{stim})$: 41% ± 6%) (**FIG. 5A**). Interestingly, the method allowed to assess the response time of the SA node upon photoactivation of the neurons, and we found that a significant increase in HR was evoked after as few as 3-4 light pulses. Thus, the activation time was in the range of 90-120ms.(**FIG. 5B**). During this time, the series of events occurring from neuronal AP to increased automaticity in the SA cardiomyocytes must include: the activation of vesciclular NE release, its diffusion to the cardiomyocyte membrane, interaction with β-AR, activation of cAMP synthesis and PKA phosphorylation of pacemaker channels. Of all these steps, agonist dependent β-AR activation has been shown to require about 50ms, the subsequent cAMP synthesis likely requires even more time. This implies that time of NE diffusion from the neuron to the cardiomyocyte is in the order of few ms.

This result is therefore in support of the hypothesis that the sympathetic-releasing terminals are in direct contact with the 'postsynaptic' cardiomyocyte membrane.

Materials and Methods

Transgenic mice. Transgenic mice expressing cre-recombinase under the control of Tyrosine Hydroxilase (TOH) promoter were bred with B6.Cg-Gt (ROSA) 26Sortm27.1 $^{(CAG-COP4*H134R/tdTomato)\ Hze}$/J expressing mice (Jackson Lab. Bar Harbor, Maine, USA). The resulting offspring has the STOP cassette deleted in the neurons, resulting in SN expression of the hChR2 (H134R)-tdTomato fusion protein. All experimental procedures described in this manuscript have been approved by the local ethical committee and communicated to the relevant Italian authority (Ministero della Salute, Ufficio VI), in compliance of Italian Animal Welfare Law (Law n 116/1992 and subsequent modifications).

Tissue samples and confocal image analysis. The sympathetic ganglia neurons has been harvested from TOHcre/loxPChR2 transgenic mice, as well as control mice, fixed in 2% paraformaldehyde (PFA) (Sigma) for 15 minutes at room temperature, equilibrated in sucrose gradient at 4°C, frozen in liquid nitrogen. Ten-micron ganglia sections have been obtained with a cryostat (Leica cardiomyocyte1850, Leica Microsystems GmbH, Wetzlar, Germany) and processed for histological and immunofluorescence analyses. Sympathetic ganglia sections have been analyzed at the confocal microscope Leica SP5.

In vivo stimulation of ChR2 expressing SGN. Mice have been anesthetized, intubated and ventilated as previously described. Stellate ganglia have been exposed and different areas have been stimulated fiber optic of different size (from 200 μm to 1 mm of diameter) powered by a LED emitting light at 470 nm (470nm LED, 1, 5 A, Thorlabs). ECG recording and LED control have been performed with an ECG-recording system (Powerlab 8/30, Bioamp and Chart 7.1 software; AD Instruments). Duration of P-waves, PQ intervals and QRS complexes have been evaluated with Chart software and ECG analysis module (AD Instruments).

FIGURE 1

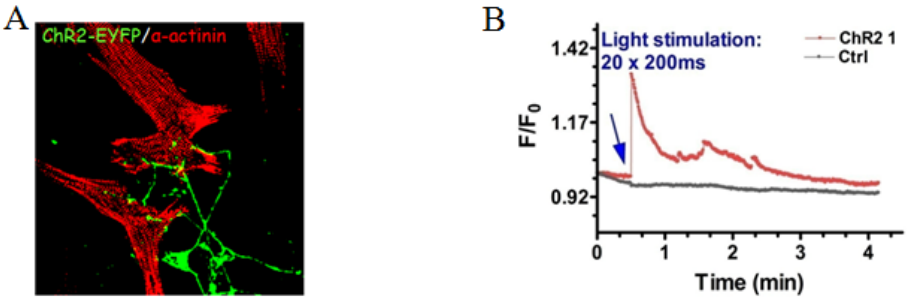

Figure 1. PC12 expressing ChR2 cells show intracellular Ca^{2+}increase upon photostimulation. A. Representation of a PC12-CM co-cultures. PC12 cells express the proteinChR2 fused with a green fluorescent protein (green signal). The CM are stained with an antibody to α-actin (red signal). **B.** Intracellular Ca^{2+} variation in ChR2 expressing PC12 cells upon stimulation with blue light. Intracellular Ca^{2+} increase was assessed with the Ca^{2+} indicator FURA2-AM, as normalized ratio between the fluorescence intensity at 340 nm and 380 nm. Red line represenr PC12 exressing ChR2, the grey line represent the cell without exogenous protein

FIGURE 2

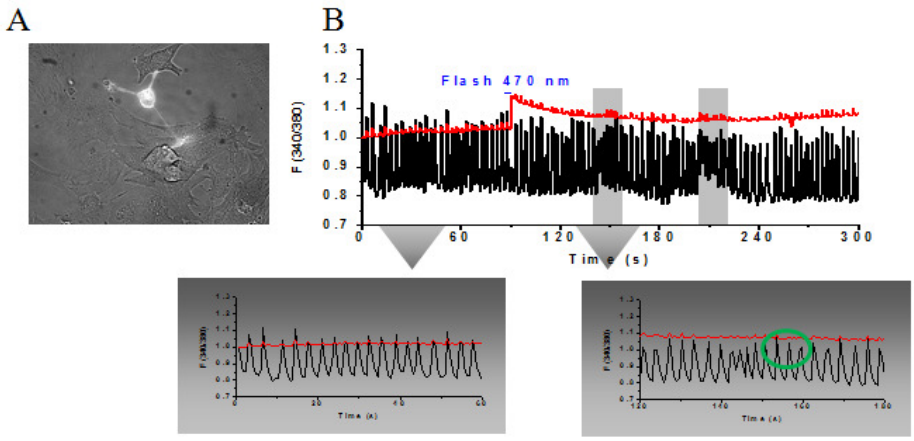

Figure 2. Variation in the CM contraction rate upon photostimulation of the coupled PC12 expressing ChR2. A. Representative image of differentiated PC12 cells expressing Chr2 interacts with co-cultured CM. **B.** Representative graph of intracellular Ca^{2+} variation assessed by FURA2-AM, in PC12 cells (red line) and in the coupled CM (black line). Upon light stimulation (flash 470 nm) we observed intracellular Ca^{2+} increse in PC12 cells and increase in the cardiac contraction rate in the target CM. Magnifications show the CM physiological contraction rate before photostimulation (left), and the variation in the CM Ca^{2+} wave after photostimulation (right).

FIGURE 3

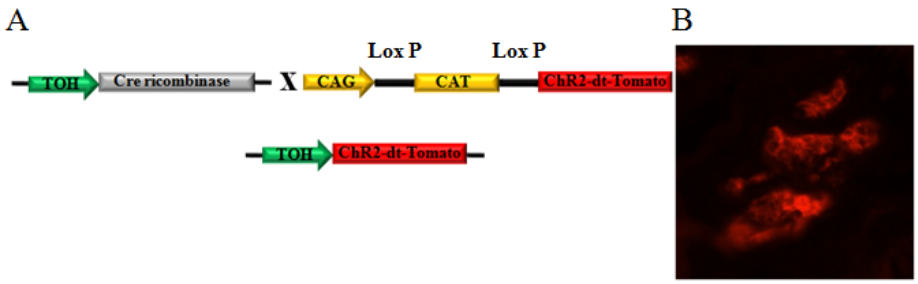

Figure 3. Generation of transgenic mice expressing ChR2 in the SN. A. Scheme of the generation of transgenic mice. Transgenic mice expressing cre-recombinase under the control of Tyrosine Hydroxilase (TOH) promoter were breeded with B6.Cg-Gt(ROSA)26Sor$^{tm27.1(CAG-COP4*H134R/tdTomato)Hze}$/J expressing mice. The resulting offspring has the STOP cassette deleted in the neurons, resulting in SN expression of the hChR2(H134R)-tdTomato fusion protein **B.** Confocal image of a cryoslice of SGN harvested from TOH-ChR2 mice. The proteins localize in the plasmamembrane of the cells as reported in literature.

FIGURE 4

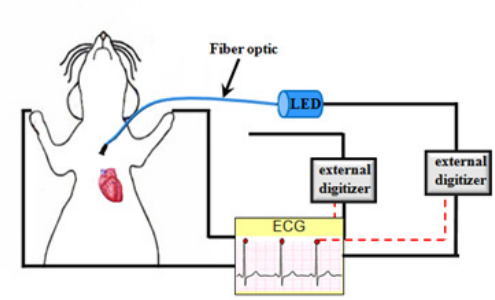

Figure 4. Schematic representation of the setup to photostimulate SN recording the ECG. Mouse were anesthetized and connected to electrods for ECG recording. LED stimulation occurs through fiber optic, and it connected through external digitalizer to the ECG apparatus, allowing us to syncronyze the LED stimulation with specific time point of ECG.

FIGURE 5

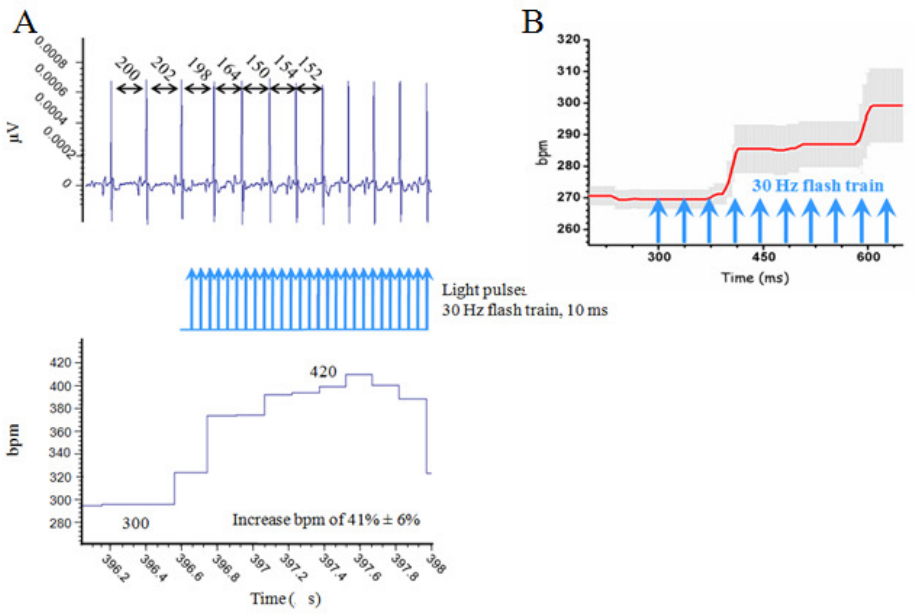

Figure 5. ECG recording of TOH-ChR2 mice upon light stimulation of stellate ganglia. A. The upper part of figure A is a representative ECG of TOH-Chr2 mice upon stimulaiton of stellate ganglia. The blue arrows represents the ligt pulses. The bottom part of figure A is the mean of the bpm during time referred to ECG. Upon ligh stimulation heart contraction rate increase, indeed the peak-to-peak distance decrese after slight pulse (upper figure): **B.** The image shows a magnification of a graph representing the avarage of ten stimulation. The clue arrows represent the light pulses. We observed increase in the heart contraction rate after four 30 Hz pulses.

Optical modulation of AP in cardiac cells

Preliminary result

In the first part of the ChR2-based study of the electrophysiological modulation of heart activity by light, we tested the feasibility of the method using rat neonatal cardiomyocytes culture as *in vitro* model.

Optical control of cardiomyocytes activity by ChR2 photostimulation *in vitro*

Recently optogenetic strategy has been used not only to modulate neuronal activity[1-4] but also to control with millisecond resolution the heart rate *in vitro* and *in vivo* [5].
Depolarization of cardiac cells triggers the opening of the L-type Ca^{2+} channels that are the initial event for the CICR process that is involved in the heart contraction.
We wanted to optically modulate the heart activity with high temporal precision and in non invasive way in living mice. To test the feasibility of the methods we test the ChR-based approach in cardiomyocytes isolated from neonatal rats. We expressed the gene encoding for ChR2(H134R) variant fused with a fluorescence protein (EYFP) by transient transfection in rat neonatal CMs.
By whole cell patch clamp recording we monitored the action potential (AP) in the cardiac cells to verify whether we were able to modulate cardiac activity by light. We stimulated ChR2 expressing CM with an LED emitting light at 470 nm, during the AP recording. CM contract spontaneously, and we observed that depending on when the light pulses was given we were able to trigger or a delay after depolarization (DADs), an early after depolarization (EAD) or a normal beat. If the light pulses was given before the ending of the repolrarization we trigger an EAD, on the contrary if we stimulated the cells before the beginning of the depolarization we trigger a DAD.
It has been shown that asynchronous oscillation in the AP are involved in the arrhythmias triggering, indeed it has been shown that the triggering of arrhythmic events could be DAD or EAD.

Because the fact that AP activation trigger the opening of the voltage-gated Ca^{2+} channel leading to the increase in the intracellular Ca^{2+} , we assessed cytosolic Ca^{2+} variation in ChR2 expressing cells upon stimulation with light at 470 nm. To monitor the variation of the concentration of the intracellular Ca^{2+} we loaded the cells with the Ca^{2+} indicator FURA2-AM (2.5 μM, 30 min). In a CM expressing the ChR2 protein we activate the action potential and we monitor intracellular Ca^{2+} variation.

We observed intracellular Ca^{2+} increase in cells expressing ChR2 upon optical stimulation with blue light, demonstrating that ChR2 phostostimulation induces an AP sufficient to open the voltage-gated Ca^{2+} channel triggering the CICR process. It is interesting to notice that the Ca^{2+} diffuses through the adjacent cells. Indeed upon stimulation of ChR2 expressing cells, intracellular Ca^{2+} increases and monitoring Ca^{2+} variation in the adjacent cells, we observed Ca^{2+} variation in the non-transfected adjacent cells. This event could be explained by the fact that CM are electrically connected one to the other with the *gap Junction*, allowing the passage of the AP originated in the ChR2 expressing cells also to the neighboring cells, leading the opening of the Ca^{2+} channel and as consequence intracellular Ca^{2+} increase also in the non-transfected cells.

Here we have been provided preliminary data showing that optical activation of ChR2 is a useful method to modulate action potential and Ca^{2+} transient in cardiac cells. We used this approach to calculate the fraction of asynchronous cells needed to trigger an arrhythmic event.

FIGURE 1

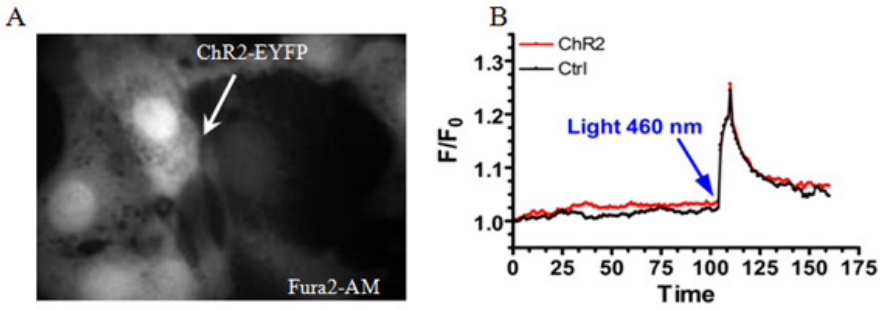

Figure 1: Mesurament of intracellular Ca^{2+} variation in neonatal cardiomyocytes upon ChR2 photostimulation assessed with the intracellular Ca^{2+} indicator FURA2-AM. A. Cultured neonatal cardiomyocytes loaded with FURA2-AM. The arrow indicates the ChR2 expressing cells. **B.** Graph represented the normalized fluorescence variation of FURA2-AM. Increase in the fluorescence intensty represent the increase in the intracellular Ca^{2+} . Upon light stimulation we were able to trigger intracellular Ca^{2+} increase due to a light-induced depolarization of membrane potential.

FIGURE 2

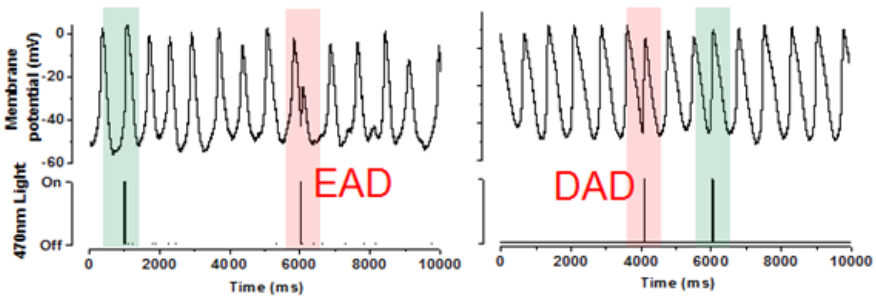

Figure 2: Optical modulation of neonatal cardiomyocytes AP using whole cell patch clamp recording. Graph represented the membrane potential variation of neonatal cardiomyocytes. Black bars represent the light pulses. Cardiomyocytes contract spontaneusly, and depending on when the light pulses was given we were able to trigger a normal beat (green bars), a EAD or DAD (red bars)

Optogenetic interrogation of the arrhythmic mechanisms in the early phase of myocardial ischemia

Abstract

Lethal ventricular arrhythmias, including sustained ventricular tachycardia (VT) and, in particular, ventricular fibrillation (VF) during the early phase of myocardial infarction, are the immediate cause of sudden cardiac dead (SCD).

Experimental studies indicate that ischemia- or infarction-induced heterogeneities in excitability, refractoriness and/or conduction create the substrate and that ectopic excitation by a variety of mechanisms may provide the extrasystoles that trigger lethal ventricular arrhythmias.

We have implemented a novel arrhythmia assay exploiting cardiac photostimulation of ChR2-expressing hearts. The method uses a fiber optic to deliver time controlled pulses of 470nm light to the epicardial surface in an open-chest anesthetized mouse.

We optically stimulate both the right atria (RA) and the ventricle. RA stimulation triggers increase in the heart rate, on the contrary photostimulation of 100 μm x 100 μm wide region epicardial region trigger a premature ventricle complex (PVC).

We triggered VT in a pro-arrhythmic condition such as AMI. We triggered sustained VT by stimulating peri-infarct area, observing an increase in the refractoriness to depolarization.

This novel approach allow us to calculate the critical mass necessary to trigger a premature ventricle beat in the order of 50 cells. Depolarization of such limited region is sufficient to trigger a sustained ventricular fibrillation in the early phase of acute myocardial ischemia.

Introduction

Lethal ventricular arrhythmias, including sustained ventricular tachycardia (VT) and, in particular, ventricular fibrillation (VF), are the immediate cause of cardiac arrest in most of the estimated 300,000 to 350,000 cases of sudden cardiac death (SCD) that occur annually in the United States of America (USA) [6, 7]. A major cause of SCD is coronary artery disease, during both the acute ischemic phase and during the infarct evolution phase. AMI induced-VF leads to SCD as the first manifestation of a preexisting coronary artery disease in about 80,000 people per year [6, 7].

Experimental studies indicate that ischemia- or infarction-induced heterogeneities in excitability, refractoriness and/or conduction create the substrate and that ectopic excitation by a variety of mechanisms may provide the extrasystoles that trigger lethal ventricular arrhythmias[8].

Many SCDs from VT/VF occur during acute myocardial ischemia [8]. Abrupt cessation of myocardial blood flow causes *Ionic imbalances* across the cardiomyocyte membrane, including H^+, Na^+, Ca^{2+} and K^+, with altered function of ion channels and transporters. In the vast majority of cases, Phase 1A arrhythmias appear to arise from reentry and manifest as bursts of VTs that rarely evolve into VF. In contrast, Phase 1B arrhythmias may emerge from both focal as well as non-focal sources and both abnormal automaticity as well as reentry may take place. Conceivably, a combination of the higher propensity to generate Ca^{2+} dependent DAD and the increased electrical resistance between cardiomyocytes in the acutely ischemic myocardium are the initiating events of conducted extra beats [9].

The factors that determine whether a DAD results in a propagating action potential in the setting of acute myocardial ischemia. Although spontaneous Ca^{2+} waves occur in buffer-perfused isolated heart preparations under physiological conditions as well as following injury [10-13], it is not known whether Ca^{2+} waves trigger arrhythmias under ischemic conditions because reduced intercellular coupling would diminish the opposing, i.e. repolarizing, effect of passive outward current generated by neighboring cardiomyocytes.

The critical mass of cells necessary to generate a conducted beat has not been identified directly. Simulation modeling indicates that in the intact non-ischemic myocardium the minimal myocardial tissue volume that needs to simultaneously depolarize to generate an extra beat is in the order of 800.000 cells.

One of the experimental ways to address selectively the mechanism of propagation of DAD and EAD uses timely and spatially controlled electrical pulses to assess the vulnerability to AP propagation in the tissue [14]. However, this system lead to production

of toxic gases, such as H_2, O_2 or Cl_2 and modification in the pH . Thus this kind of approach could be used only for brief depolarization that trigger AP and not for prolonged stimulation.

Thus our aim is to used optogenetic approach to modulate non invasively and in alimited region of the heart the AP of the cardiac cells.

Optical control of heart rate by ChR2 photostimulation in living mice

We have implemented a novel arrhythmia assay capable of high spatial resolution and temporal accuracy, that uses cardiac photostimulation of ChR2-expressing hearts. The methodology allowed to determine the critical tissue mass and the vulnerability to generate sustained VT/VF in the normal myocardium and during acute myocardial ischemia.

ChR2 is a photoactivatable microbial derived cation channel, mostly permeable to Na^+. Its structural similarity with rhodopsin confers the proteins the property of undergoing a conformational change upon illumination, which results in the immediate change of ionic permeability [15]. ChR2 exhibits fast temporal kinetics (in the order of ms) that make it possible to drive reliable trains of high frequency action potentials in vivo [2, 16]. ChR2 has mostly been used in neurons allowing optical 'interrogation' of a specific neural circuit *in vivo* [3], and it has been shown to work in other excitable tissues including the myocardium.

To achieve ChR2 expression in cardiac cells, we crossed B6.Cg-Gt (ROSA) 26Sortm27.1 $^{(CAG-COP4*H134R/tdTomato)\ Hze}$**/J** expressing mice with mice expressing Cre recombinase under control of the cardiac αMHC promoter. The resulting offspring has the STOP cassette deleted in the heart, resulting in expression of the hChR2(H134R)-tdTomato fusion protein, which localizes in the cardiomyocyte membrane as expected (**fig 1A**). The hearts had normal histology (**fig 1B**) with unchanged HR and function when compared to $Cre^+/ChR2^-$ or $Cre^-/ChR2^+$ or normal controls.

A fiber optic was used to deliver time controlled pulses of 470 nm light to the epicardial surface in open-chest anesthetized ChR2 mice. Placement of the fiber tip through a micromanipulator under stereo-microscope guide allowed photostimulation of a spatially defined region of the heart. During the experiment, the cardiac activation sequence is continuously monitored through surface ECG, and online detection of R-waves allows to regulate timing of the light pulses with respect to the spontaneous QRS.

Epicardial illumination with a time controlled pulse of light at 470nm was effective in depolarizing a confined area of myocardium. Atrial pacing from both RA and LA was obtained at rates up to 900 bmp, (5ms light pulses delivered at 15Hz) (preliminary data **FIG. 1C**), demonstrating that spatially regulated stimulation of the atria was achieved.

Consistent with previus report [5] the delay between the light pulse and the ECG respose in the atria is 13.5 ms ± 5.6 (mean ±SEM, n=6) and the delay from the light pulse to the onset of the ventricle extrabeat is 9.4 ms ± 0.5 ms (mean ± SEM, n=9).

We used differently-sized fibers (from 200 µm to 700 µm core size) for ventricular photoactivation analyzing the probability to generate a PVC (**FIG. 1D**) to determine the critical myocardial mass to generate a globally spreading depolarization wave.

We observed that stimulation of 100 µm x 100 µm wide area is sufficent to conduct light-induced beats to the whole heart, increasing the capture efficiency with the enlargement of the stimulated areas, reaching the maximum with the 700 µm sized fiber (**FIG 2A**). Thus we determined that photoactivation was achieved in a region corresponding to around 50 cells of the first epicardial layer (**FIG. 2B**). Because the fact that fiber optic drive light deep in the tissue we estimated the volume of the cells activated by light considering a depth of 200 µm and with a 100 µm x 100 µm wide region. In this condition the volume of cardiac cells depolarized by light is 0.010 mm^3.

The surface threshold of myocardial photostimulation was evaluated with respect to the latency of the light pulse from the preceeding QRS. Within 40 ms from the R-wave onset (which would correspond to EAD events, the probability of generating a PVC and the minimal critical tissue mass higher when compared to pulses falling in the diastolic phase, mimicking the effect of a DAD.

We test optogenetic approach also in a pro-arrhythmic condition such as AMI. Indeed it has been demonstrated that the risk of ventricular fibrillation is common in the early phase of acute myocardial infarction [17, 18].

Acute coronary ischemia was obtained by legating the left anterior descendant (LAD) coronary artery [19] during continuous ECG monitoring. The tributary myocardium became immediately pale and within the first ten minutes, ischemia caused alteration in the QRS complex and amplitude, with only rare ectopic ventricular beats. Injured area size was confirmed by using tatrazolium staining as shown in figure **FIG. 3A**.

Photostimulation was obtained with 1s bursts of pacing flashes on the left ventricle at the infarct border zone and in the right ventricle close to the right ventricular outflow tract (RVOT). Stimulations evoked monomorphic VT, that had a capture ratio of about 1:1.3 at frequencies up to 20 Hz compare to 1:1 of the control, indicating that the refractoriness to depolarization increased during phase 1A of ischemia.

After 15-30 min of ischemia, burst photostimulation evoked frequent episodes of ventricular flutter and rare VF, which terminated promptly at the end of pacing , with a pause to the subsequent beat. Stimulation of the RV caused the pacing-evoked VT to be sustained after pacing cessation, frequently lasting a limited number of beats . At frequencies 16-25 Hz, burst stimulation triggered frequently sustained polymorphic VT/VF lasting 8-50 s (**FIG. 3B**), which was highly reproducible in the same heart, but differed in optimal train rate and illumination position among different experiments.

To conclude, we calculated the critical mass necessary to trigger a PVC was around 0.01 mm^3 that are less than 1000 cells. Moreover we observed that the refractoriness to depolarization of in the acute phase of myocardial ischemia is increased and light induced DADs in a 100 µm x 100 µm wide area is sufficient to trigger a sustained VT.

Material and Methods

Transgenic mice. Transgenic mice expressing cre-recombinase under the control of alpha-Myosin Heavy Chain (α-MHC) promoter were breeded with B6.Cg-Gt (ROSA) 26Sortm27.1 $^{(CAG-COP4*H134R/tdTomato)\ Hze}$/J expressing mice (Jackson Lab. Bar Harbor, Maine, USA). . The resulting offspring has the STOP cassette deleted in the heart, resulting in cardiac expression of the hChR2(H134R)-tdTomato fusion protein. All experimental procedures described in this manuscript have been approved by the local ethical committee and communicated to the relevant Italian authority (Ministero della Salute, Ufficio VI), in compliance of Italian Animal Welfare Law (Law n 116/1992 and subsequent modifications).

Tissue samples and confocal image analysis. The heart has bee harvested from αMHCcre/loxPChR2 transgenic mice, as well as control mice, fixed in 2% paraformaldehyde (PFA) (Sigma) for 15 minutes at room temperature, equilibrated in sucrose gradient at 4°C, frozen in liquid nitrogen. Ten-micron myocardial sections have been obtained with a cryostat (Leica CM1850, Leica Microsystems GmbH, Wetzlar, Germany) and processed for histological and immunofluorescence analyses. Heart sections have been analyzed at the confocal microscope Leica SP5.

Myocardial infarction. Adult transgenic and control mice have been anesthetized either by isofluorane (1.5% O2) or Avertin administration (250mg/kg i.p.) and fixed in the supine position. Mice have been intubated with a 24G needle and ventilated with room air (tidal volume 0.4ml; 120 strokes/min) using an artificial ventilator (SAR-830) and both temperature and respiratory rate have been monitored constantly. The skin has been dissected by a lateral 1.5 cm cut at the sub-ascellary region. The subcutaneous muscles have been removed and a 0.5 cm incision have been performed at the level of the fourth intercostal space. Self-retaining microretractors have been then used to separate the 3rd and 4th ribs enough to get adequate exposure of the operating region, but the ribs were kept intact. The left ventricular wall has been exposed and once identified, the main trunk of the left descending coronary artery has been ligated by using a 7/0 polypropylene suture.

Calculation of critical mass of cardiac cells. Mouse heart was harvested and loading with the mitochondrial dye TMRM (xxx) and was examined at confocal microscope

Triphenyl-Tretrazolium staining. Hearts have been removed four hours upon myocardial infarction. Two mm myocardial slices have been stained in 1% tetrazolium (Sigma) in phosphate buffer at 37% for 20 min. at 37°C. The slices have been washed in the buffer and images of the sections have been taken with a xxx camera for later analysis of infarct size.

Photoactivation of the myocardium and ECG recording in anesthetized mice. Mice have been anesthetized, intubated and ventilated as previously described. Hert have been exposed and different areas have been stimulated with a fiber optic of different size (from 200 μm to 1 mm of diameter) powered by a LED emitting light at 470 nm (470nm LED, 1,5 A, Thorlabs). ECG recording and LED control have been performed with an ECG-recording system (Powerlab 8/30, Bioamp and Chart 7.1 software; AD Instruments). Duration of P-waves, PQ intervals and QRS complexes have been evaluated with Chart software and ECG analysis module (AD Instruments).

Statistical analysis. All data are expressed as the mean±s.e.m. Comparison between the experimental groups has been performed by using the non-paired Student's *t* and Anova tests with $P<0.05$ being considered statistically significant.

FIGURE 1

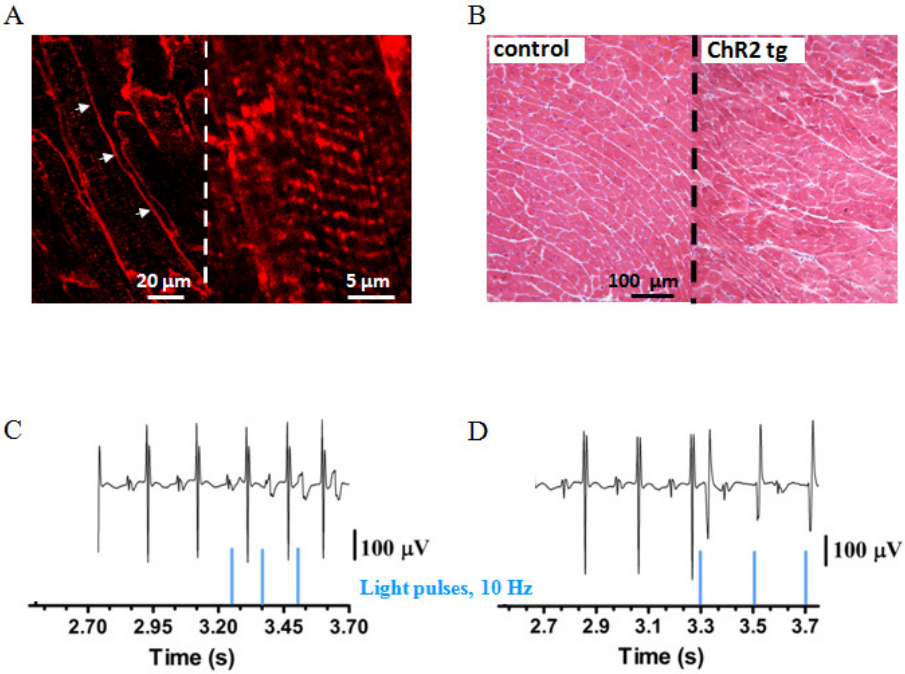

Figure 1: ChR2 photostimulation of a limited region of the heart is sufficent to modulate heart activity A. Heart were hervasted from ChR2 expressing mice and fix in PFA 2%. It was freeze and 20 micron cryosection were performed. Cryosection were analyzed at the confocal microscope (LEICA SP5XXX) The protein was expressed in cardiac cells and correctly localized the membrane of cardaic cells. In the magnification it is clear the localization of the protein in the t-tubes. **B**. As shown in the hematoxilin and eosin staining hearts expressing ChR2 do not present singal of fibrosis or differences cardiac cells size compare to the control. Using optic fibers of different diameter we were able to stimulate heart in different region. AS shown in panel **C,** light-induced atrial pacing from both RA and LA was obtained at rates up to 900bmp, (5ms light pulses delivered at 15Hz) demonstrating that spatially regulated stimulation of the atria was achieved. **D.** As show in this representative ECG of epicardial pacing, ventricular photoactivation of an epicardial area with 20 mW/mm^2 light was sufficient to trigger a premature conducted beats, with a minimal size cutoff in the order of 200 µm, when pulses were delivered after 30 ms from the R-wave onset

FIGURE 2

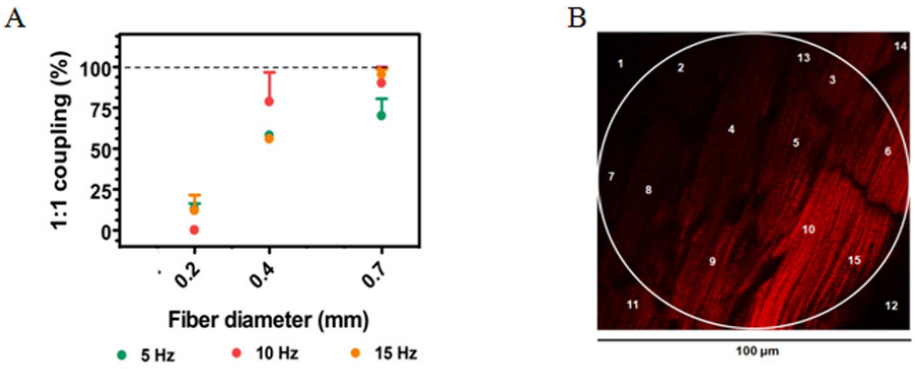

Figure 2: The critical mass necessary to trigger an arrhythmic beat is around 50 cells. A. Fiber optic are powered by LED emitting light at 470 nm. We tested fiber optic of different size to verify which is mass of cells necessary to trigger an arrhythmic event. In parallel we verfy the train pulses frequency that trigger premature beats in a beats over pulses ratio 1:1. As shown in panel **A** 400 µm fiber optic (green trace) and 1 mm fiber optic (red trace) trigger premature beats in beats/ratio 1:1 at 10 Hz and 15 Hz ,respectively. 200 µm fiber stimulates a too small region to trigger beats conducted to the entire heart. We concluded that it necessary 200 µm * 200 µm wide region to conduct the arrhythmic beat to the entire myocardium. We calculate the number of cells depolarized by the fiber optic. We hervasted heart from wt mouse and we loaded it TMRM. We acquire confocal image of a regionof epicardial layer. As shown in panel **B** we consider a round area (white circle) of 100 µm and we estimated the amount of cells or portion of cells around 12. Consider a region of 200 µm of diameter the number of cells will be around 50 cells.

FIGURE 3

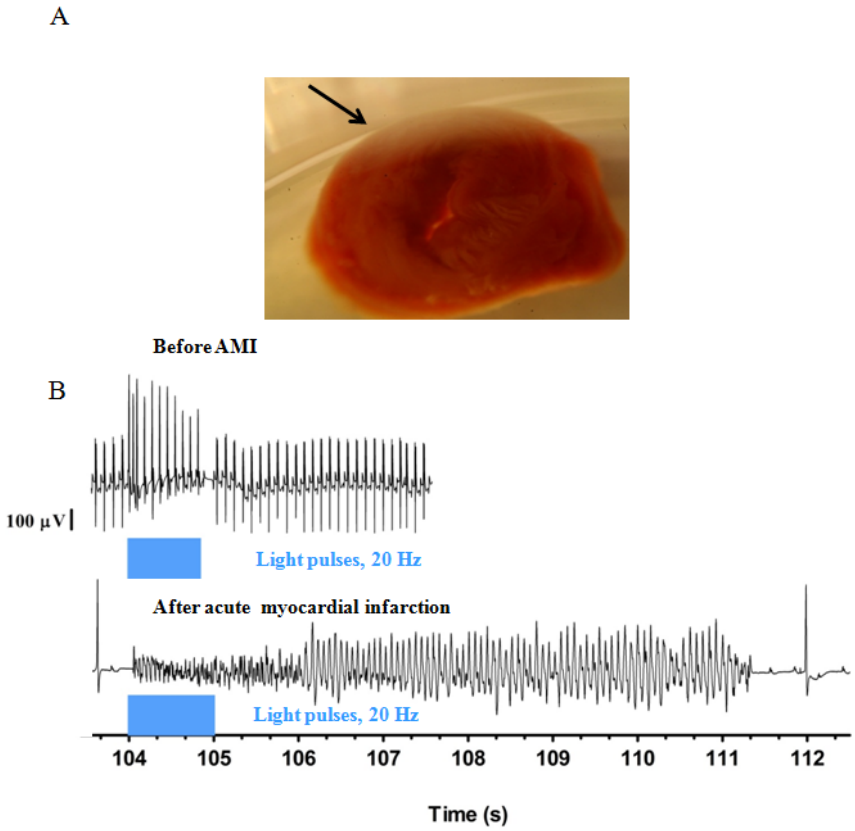

Figure 3: Photostimulation of ChR2 expressing heart before and after AMI. A. Image of a section of infarcted heart loaded with triphenyl tetrazolium chloride to monitor the size of injury. The lighter part of the heart section represent the injured region. **(B).** Fifteen minutes after AMI we depolarized with 20 Hz light pulses peri-infarct zone, observing that by depolarizing a limited fraction of cells we were able to trigger a sustained ventricular tachycardia that is prolonged even after the light pulses. Stimulations evoking monomorphic VT had a capture ratio of about 1:1.3 at frequencies up to 20 Hz, indicating that the refractoriness to depolarization increased during phase 1A of ischemia. Photostimulation of left ventricle before AMI was performed as control.

REFERENCES

1. Zhang F Fau - Wang, L.-P., et al. (2006 Oct) *Channelrhodopsin-2 and optical control of excitable cells*. Nat, Methods
2. Boyden Es Fau - Zhang, F., et al. (2005 Sep) *Millisecond-timescale, genetically targeted optical control of neural activity*. Nat, Neurosci.
3. Zhang F Fau - Wang, L.-P., et al. (2007 Apr 5) *Multimodal fast optical interrogation of neural circuitry*. Nature, .
4. Arenkiel Br Fau - Peca, J., et al. (,2007 Apr 19) *In vivo light-induced activation of neural circuitry in transgenic mice expressing channelrhodopsin-2*. Neuron.
5. Bruegmann T Fau - Malan, D., et al. (2010 Nov) *Optogenetic control of heart muscle in vitro and in vivo*. Nat, Methods.
6. Zipes Dp Fau - Wellens, H.J. and H.J. Wellens, *Sudden cardiac death.* Circulation, x, 1998 Nov 24(0009-7322 (Print)).
7. Rubart M Fau - Zipes, D.P. and D.P. Zipes (2005 Sep) *Mechanisms of sudden cardiac death*. J. Clin Invest
8. Huikuri Hv Fau - Castellanos, A., R.J. Castellanos A Fau - Myerburg, and R.J. Myerburg, *Sudden death due to cardiac arrhythmias.* N. Engl J Med 2001 Nov 15(0028-4793 (Print)).
9. Verkerk Ao Fau - Veldkamp, M.W., et al., *Effects of cell-to-cell uncoupling and catecholamines on Purkinje and ventricular action potentials: implications for phase-1b arrhythmias.* Cardiovasc, Res 2001 Jul(0008-6363 (Print)).
10. Wier Wg Fau - ter Keurs, H.E., et al., *Ca2+ 'sparks' and waves in intact ventricular muscle resolved by confocal imaging.* Circ, Rest, 1997 Oc(0009-7330 (Print)).
11. Baader Ap Fau - Buchler, L., et al. (Res 2002 Jan) *Real time, confocal imaging of Ca(2+) waves in arterially perfused rat hearts*. Cardiovasc, Res.
12. Tanaka H Fau - Oyamada, M., et al., *Excitation-dependent intracellular Ca2+ waves at the border zone of the cryo-injured rat heart revealed by real-time confocal microscopy.* J. Mol Cell Cardiol 2002 Nov(0022-2828 (Print)).
13. Kaneko T Fau - Tanaka, H., et al., *Three distinct types of Ca(2+) waves in Langendorff-perfused rat heart revealed by real-time confocal microscopy.* Circ, Res 2000 May 26(1524-4571 (Electronic)).
14. Wikswo Jp Jr Fau - Lin, S.F., R.A. Lin Sf Fau - Abbas, and R.A. Abbas, *Virtual electrodes in cardiac tissue: a common mechanism for anodal and cathodal stimulation.* Biophys, J. x, Biophys, J. 1995 Dec(0006-3495 (Print)).
15. Nagel G Fau - Szellas, T., et al. (2003 Nov 25) *Channelrhodopsin-2, a directly light-gated cation-selective membrane channel*. Proc Natl Acad Sci, U. S. A. .
16. Nagel G Fau - Brauner, M., et al., *Light activation of channelrhodopsin-2 in excitable cells of Caenorhabditis elegans triggers rapid behavioral responses.* Curr, Biol 2005 Dec 20(0960-9822 (Print)).
17. Campbell Rw Fau - Murray, A., D.G. Murray A Fau - Julian, and D.G. Julian, *Ventricular arrhythmias in first 12 hours of acute myocardial infarction. Natural history study.* Br Heart, J. , 1981 Oct(0007-0769 (Print)).
18. Adgey Aa Fau - Devlin, J.E., et al. (1982 Jan) *Initiation of ventricular fibrillation outside hospital in patients with acute ischaemic heart disease*. 1982 Jan.

19. Johnston Km Fau - MacLeod, B.A., M.J. MacLeod Ba Fau - Walker, and M.J. Walker, *Responses to ligation of a coronary artery in conscious rats and the actions of antiarrhythmics.* Can, J. Physiol Pharmacol 1983 Nov(0008-4212 (Print)).

SUPPLEMENTARY DISCUSSION AND CONCLUSION

In the first part of this work, using SN-CM co-cultures as *in vitro* model, we have been provided evidence of the existence of a restricted and specialized domain between SN and CM with high concentration of NT. Previous studies have only been speculate on the existence of the synaptic interaction between SN and CM [43-46], without any specific demonstration of the functional role of this close relation in the CM intracellular signalling. Here we have been used a FRET-based approach in order to monitor β-ARs activation upon SN stimulation mimicking the release of NE during the *flight or fight* response. The evidence of the existence of synaptic connections between SN and CM are the following: (a) SN stimulation induces increase in the intracellular cAMP and PKA activity only in the innervated CM. (b) Perfusing SNs with the stimulation solution we washed away the aspecific release of NE, observing the response only due to the NT acting in a confined domain. Activation of SN with the bathing solution triggers the response only in the target cells. (c) Using the non specific β-blocker propranolol (PROPR.) we showed that the [PROPR.] needed to block the SN-induced response is higher than that needed to abolish the response induced by 3.5e-10 M of NE which trigger a FRET variation similar to that induced by SN. This implies that NE released act in a domain in which the concentration is high and it is not aspecifically dilute in the medium.

The existence of a synaptic connection between SNs and the CMs is important in the studying of arrhythmic event. Indeed it has been suggested that unbalanced SN discharge is a cause of arrhythmic event in healthy and diseased heart[50], and it has been shown that NE spillover leads to arrhythmic event in the failing myocardium[52]. In addition recently it has been suggested that stimulation of a limited region of the cells by NE is sufficient to trigger a premature ventricle complex [56]. Taking into account all this consideration the existence of synaptic contact between SN and CM, suggests that the unbalanced impairment in the SN could lead to a depolarization in a limited group of cells that represents the critical mass sufficient to trigger a premature ventricle beat.

Indeed, the aims of the second and the third parts of the work are to investigate on the role of the SNS in the arrhythmias triggering, and to understand which is the critical mass

necessary to induce a premature ventricle beat *in vivo*. We based our strategy on the ChR-microbial proteins, in particular ChR2 that is a light gated cation channel, becoming permeable mostly to Na^+ upon light stimulation at 470 nm[68]. Using transgenic mice expressing ChR2 in adrenergic neurons we were able to increase heart contraction rate non invasively and with millisecond resolution *in vivo*. We showed that increasing in the heart frequency occurs after 100-150 ms from light stimulation, supporting the hypothesis of the existence of SN-CM synapses.

Using another model of transgenic mice that express ChR2 in the cardiac cells we are investigating on the critical mass necessary to trigger an arrhythmic event. We were able to increase the heart rate by pacing a limited region of the atria (from 200 µm to 1 mm, diameter). Moreover photostimulating a region of 200 µm of diameter in the ventricle we were able to trigger a premature ventricle beat, suggesting that depolarization of 100 x 100 mm wide region of epicardial cells is sufficient to generate an arrhythmic beat that is conducted in the whole heart.

Thus in this work we provided evidence of the existence of synaptic contact between SNs and CMs *in vitro*, supported by preliminary *in vivo* experiments, showing that the control of heart activity by sympathetic neurons occurs in fraction of time (100-150 ms) that is compatible to 30-50 nm of ST-to-CM distance. In addition we showed that by depolarizing a limited fraction of cells we were able to trigger an arrhythmic beat that is conducted in the whole heart, supporting the hypothesis previous described that the unbalanced SN impairment is a cause of an asynchronous activation of a small fraction of cells sufficient to trigger arrhythmic event.

REFERENCES

1. Arora, R.C., et al. (2003) *Intrinsic cardiac nervous system in tachycardia induced heart failure*. Am J Physiol Regul Integr Comp Physiol **285**, R1212-23 DOI: 10.1152/ajpregu.00131.2003.
2. Esler M Fau - Jennings, G., et al. (1988) *Assessment of human sympathetic nervous system activity from measurements of norepinephrine turnover*. Hypertension, .
3. Shcherbakova, O.G., et al. (2007) *Organization of beta-adrenoceptor signaling compartments by sympathetic innervation of cardiac myocytes*. J Cell Biol **176**, 521-33 DOI: 10.1083/jcb.200604167.
4. Zhang F Fau - Wang, L.-P., et al. (2006 Oct) *Channelrhodopsin-2 and optical control of excitable cells*. Nat, Methods
5. Zhang F Fau - Wang, L.-P., et al. (2007 Apr 5) *Multimodal fast optical interrogation of neural circuitry*. Nature, .
6. Shimada T Fau - Kawazato, H., et al. (2004 Oct) *Cytoarchitecture and intercalated disks of the working myocardium and the conduction system in the mammalian heart*. Anat Rec, A. Discov Mol Cell Evol Biol
7. Sheikh F Fau - Ross, R.S., J. Ross Rs Fau - Chen, and J. Chen (2009 Aug) *Cell-cell connection to cardiac disease*. Trends Cardiovasc, Med.
8. Jamora C Fau - Fuchs, E. and E. Fuchs (Nat Cell, Biol 2002 Apr) *Intercellular adhesion, signalling and the cytoskeleton*. Nat Cell,x.
9. Yamada S Fau - Pokutta, S., et al. (2005 Dec 2) *Deconstructing the cadherin-catenin-actin complex*. Cell, .
10. Severs Nj Fau - Bruce, A.F., et al. (2008 Oct 1) *Remodelling of gap junctions and connexin expression in diseased myocardium*. Cardiovasc, Res
11. Anderson Rh Fau - Yanni, J., et al. *The anatomy of the cardiac conduction system*. Clin, Anat.
12. Fabiato A Fau - Fabiato, F. and F. Fabiato (1975 Aug) *Contractions induced by a calcium-triggered release of calcium from the sarcoplasmic reticulum of single skinned cardiac cells*. J. Physiol.
13. Berridge, M.J. (2003 Oct) *Cardiac calcium signalling*. Biochem Soc, Trans
14. Chen-Izu Y Fau - McCulle, S.L., et al. (2006 Jul 1) *Three-dimensional distribution of ryanodine receptor clusters in cardiac myocytes*. Biophys, J.
15. Yatani A Fau - Codina, J., et al. (, 1987 Nov 27) *A G protein directly regulates mammalian cardiac calcium channels*. Science, .
16. Hulme Jt Fau - Lin, T.W.C., et al. (2003 Oct 28) *Beta-adrenergic regulation requires direct anchoring of PKA to cardiac CaV1.2 channels via a leucine zipper interaction with A kinase-anchoring protein 15*. Proc Natl Acad Sci, U. S. A. .
17. Reiken S Fau - Lacampagne, A., et al. (2003 Mar 17) *PKA phosphorylation activates the calcium release channel (ryanodine receptor) in skeletal muscle: defective regulation in heart failure*. J. Cell Biol.
18. Brittsan Ag Fau - Carr, A.N., et al. (2000 Apr 21) *Maximal inhibition of SERCA2 Ca(2+) affinity by phospholamban in transgenic hearts overexpressing a non-phosphorylatable form of phospholamban*. J. Biol Chem.
19. Hildreth V Fau - Anderson, R.H., et al. (2009 Jan

) *Autonomic innervation of the developing heart: origins and function*. Clin, Anat

20. Ieda M Fau - Kanazawa, H., et al. (2007 May) *Sema3a maintains normal heart rhythm through sympathetic innervation patterning*. Nat, Med
21. Snider, W.D. (1994 Jun 3) *Functions of the neurotrophins during nervous system development: what the knockouts are teaching us*. Cell, .
22. Lockhart St Fau - Turrigiano, G.G., S.J. Turrigiano Gg Fau - Birren, and S.J. Birren (2008 Jun) *Nerve growth factor modulates synaptic transmission between sympathetic neurons and cardiac myocytes*. J. Neurosci
23. Murad F Fau - Chi, Y.M., et al. *Adenyl cyclase. III. The effect of catecholamines and choline esters on the formation of adenosine 3',5'-phosphate by preparations from cardiac muscle and liver*. J. Biol Chem.
24. Sculptoreanu A Fau - Scheuer, T., W.A. Scheuer T Fau - Catterall, and W.A. Catterall (1993 Jul 15) *Voltage-dependent potentiation of L-type Ca2+ channels due to phosphorylation by cAMP-dependent protein kinase*. Nature, .
25. Yoshida A Fau - Takahashi, M., et al. (1992 Feb) *Phosphorylation of ryanodine receptors in rat myocytes during beta-adrenergic stimulation*. J. Biochem
26. Toyofuku T Fau - Kurzydlowski, K., et al. (1993 Feb 5) *Identification of regions in the Ca(2+)-ATPase of sarcoplasmic reticulum that affect functional association with phospholamban*.
27. Cao, J.M., et al. (2000) *Relationship between regional cardiac hyperinnervation and ventricular arrhythmia*. Circulation **101**, 1960-9.
28. Xiang, Y. and B.K. Kobilka (2003) *Myocyte adrenoceptor signaling pathways*. Science **300**, 1530-2 DOI: 10.1126/science.1079206.
29. Chruscinski Aj Fau - Rohrer, D.K., et al. (1999 Jun 11) *Targeted disruption of the beta2 adrenergic receptor gene*. J. Biol Chem.
30. Bernstein D Fau - Fajardo, G., et al. (Am, J. Physiol Heart Circ Physiol 2005 Dec) *Differential cardioprotective/cardiotoxic effects mediated by beta-adrenergic receptor subtypes*. Am, J. Physiol Heart Circ Physiolx.
31. Zheng M Fau - Zhu, W., et al. (2005 Dec) *Emerging concepts and therapeutic implications of beta-adrenergic receptor subtype signaling*. Pharmacol, Ther.
32. Rohrer Dk Fau - Desai, K.H., et al. (1996 Jul 9) *Targeted disruption of the mouse beta1-adrenergic receptor gene: developmental and cardiovascular effects*. Proc Natl Acad Sci, U. S. A. .
33. Devic, E., et al. (2001) *Beta-adrenergic receptor subtype-specific signaling in cardiac myocytes from beta(1) and beta(2) adrenoceptor knockout mice*. Mol Pharmacol **60**, 577-83.
34. Nikolaev Vo Fau - Moshkov, A., et al. (2010 Mar 26) *Beta2-adrenergic receptor redistribution in heart failure changes cAMP compartmentation*. Science, .
35. Nikolaev, V.O., et al. (2006) *Cyclic AMP imaging in adult cardiac myocytes reveals far-reaching beta1-adrenergic but locally confined beta2-adrenergic receptor-mediated signaling*. Circ Res **99**, 1084-91 DOI: 10.1161/01.RES.0000250046.69918.d5.
36. Meredith It Fau - Eisenhofer, G., et al. (1993 Jul) *Cardiac sympathetic nervous activity in congestive heart failure. Evidence for increased neuronal norepinephrine release and preserved neuronal uptake*. Circulation, .
37. Kiuchi K Fau - Shannon, R.P., et al. (1993 Mar) *Myocardial beta-adrenergic receptor function during the development of pacing-induced heart failure*. J. Clin Invest

38. Engelhardt S Fau - Bohm, M., et al. (1996 Jan) *Analysis of beta-adrenergic receptor mRNA levels in human ventricular biopsy specimens by quantitative polymerase chain reactions: progressive reduction of beta 1-adrenergic receptor mRNA in heart failure*. J. Am Coll Cardiol **0735-1097 (Print)**.
39. Ponsioen B Fau - Zhao, J., et al. (2004 Dec) *Detecting cAMP-induced Epac activation by fluorescence resonance energy transfer: Epac as a novel cAMP indicator*. Embo Rep
40. Zhang J Fau - Ma, Y., et al. (2001 Dec 18) *Genetically encoded reporters of protein kinase A activity reveal impact of substrate tethering*. Proc Natl Acad Sci, U. S. A. .
41. de Rooij J Fau - Zwartkruis, F.J., et al. (1998 Dec 3) *Epac is a Rap1 guanine-nucleotide-exchange factor directly activated by cyclic AMP*. Nature, .
42. Allen, M.D. and J. Zhang (2006) *Subcellular dynamics of protein kinase A activity visualized by FRET-based reporters*. Biochem Biophys Res Commun **348**, 716-21 DOI: 10.1016/j.bbrc.2006.07.136.
43. Landis, S.C. (1976 Nov) *Rat sympathetic neurons and cardiac myocytes developing in microcultures: correlation of the fine structure of endings with neurotransmitter function in single neurons*. Proc Natl Acad Sci, U. S. A.
44. Potter, D.D., et al. (1986) *Synaptic functions in rat sympathetic neurons in microcultures. II. Adrenergic/cholinergic dual status and plasticity*. J Neurosci **6**, 1080-98.
45. Zaika, O., J. Zhang, and M.S. Shapiro (2011) *Functional role of M-type (KCNQ) K(+) channels in adrenergic control of cardiomyocyte contraction rate by sympathetic neurons*. J Physiol **589**, 2559-68 DOI: 10.1113/jphysiol.2010.204768.
46. Ogawa, S., et al. (1992) *Direct contact between sympathetic neurons and rat cardiac myocytes in vitro increases expression of functional calcium channels*. J Clin Invest **89**, 1085-93 DOI: 10.1172/jci115688.
47. Marvin Wj Jr Fau - Atkins, D.L., et al. (1984 Jul) *In vitro adrenergic and cholinergic innervation of the developing rat myocyte*. Circ, Res
48. Conforti L Fau - Tohse, N., N. Tohse N Fau - Sperelakis, and N. Sperelakis (1991 Apr) *Influence of sympathetic innervation on the membrane electrical properties of neonatal rat cardiomyocytes in culture*. J. Dev Physiol.
49. Meredith, I.T., et al. (1991) *Evidence of a selective increase in cardiac sympathetic activity in patients with sustained ventricular arrhythmias*. N Engl J Med **325**, 618-24 DOI: 10.1056/nejm199108293250905.
50. Dae, M.W., et al. (1997) *Heterogeneous sympathetic innervation in German shepherd dogs with inherited ventricular arrhythmia and sudden cardiac death*. Circulation **96**, 1337-42.
51. Chen, L.S., et al. (2007) *New perspectives on the role of autonomic nervous system in the genesis of arrhythmias*. J Cardiovasc Electrophysiol **18**, 123-7 DOI: 10.1111/j.1540-8167.2006.00590.x.
52. Du Xj Fau - Cox, H.S., et al. (1999 Sep) *Sympathetic activation triggers ventricular arrhythmias in rat heart with chronic infarction and failure*.
53. Akutsu, Y., et al. (2008) *Cardiac sympathetic nerve abnormality predicts ventricular tachyarrhythmic events in patients without conventional risk of sudden death*. Eur J Nucl Med Mol Imaging **35**, 2066-73 DOI: 10.1007/s00259-008-0879-x.

54. Paul, M., et al. (2006) *Impact of sympathetic innervation on recurrent life-threatening arrhythmias in the follow-up of patients with idiopathic ventricular fibrillation*. Eur J Nucl Med Mol Imaging **33**, 866-70 DOI: 10.1007/s00259-005-0061-7.
55. Keller, N.R., et al. (2004) *Norepinephrine transporter-deficient mice exhibit excessive tachycardia and elevated blood pressure with wakefulness and activity*. Circulation **110**, 1191-6 DOI: 10.1161/01.cir.0000141804.90845.e6.
56. Myles, R.C., et al. (2012) *Local beta-adrenergic stimulation overcomes source-sink mismatch to generate focal arrhythmia*. Circ Res **110**, 1454-64 DOI: 10.1161/circresaha.111.262345.
57. Priori Sg Fau - Napolitano, C., et al. (2002 Jul 2) *Clinical and molecular characterization of patients with catecholaminergic polymorphic ventricular tachycardia*. Circulation, .
58. Priori Sg Fau - Napolitano, C., et al. (2001 Jan 16) *Mutations in the cardiac ryanodine receptor gene (hRyR2) underlie catecholaminergic polymorphic ventricular tachycardia*. Circulation, .
59. Postma Av Fau - Denjoy, I., et al. *Absence of calsequestrin 2 causes severe forms of catecholaminergic polymorphic ventricular tachycardia*. Circ Res. **18;91(8):e21-6**.
60. Bers, D.M. (2004 Aug) *Macromolecular complexes regulating cardiac ryanodine receptor function*. J. Mol Cell Cardiol.
61. Marx So Fau - Reiken, S., et al. (2000 May 12) *PKA phosphorylation dissociates FKBP12.6 from the calcium release channel (ryanodine receptor): defective regulation in failing hearts*. Cell, .
62. Wehrens Xh Fau - Lehnart, S.E., et al. (2003 Jun 27) *FKBP12.6 deficiency and defective calcium release channel (ryanodine receptor) function linked to exercise-induced sudden cardiac death*. Cell, .
63. Wehrens Xh Fau - Lehnart, S.E., et al. (2004 Apr 2) *Ca2+/calmodulin-dependent protein kinase II phosphorylation regulates the cardiac ryanodine receptor*. Circ, Res.
64. Lehnart Se Fau - Mongillo, M., et al. (2008 Jun) *Leaky Ca2+ release channel/ryanodine receptor 2 causes seizures and sudden cardiac death in mice*. J. Clin Invest
65. Jiang D Fau - Xiao, B., et al. (2004 Aug 31) *RyR2 mutations linked to ventricular tachycardia and sudden death reduce the threshold for store-overload-induced Ca2+ release (SOICR)*. Proc Natl Acad Sci, U. S. A. .
66. George Ch Fau - Higgs, G.V., F.A. Higgs Gv Fau - Lai, and F.A. Lai (2003 Sep 19) *Ryanodine receptor mutations associated with stress-induced ventricular tachycardia mediate increased calcium release in stimulated cardiomyocytes*. Circ, Res.
67. Leenhardt A Fau - Lucet, V., et al. (1995 Mar 1) *Catecholaminergic polymorphic ventricular tachycardia in children. A 7-year follow-up of 21 patients*. Circulation, .
68. Nagel G Fau - Szellas, T., et al. (2003 Nov 25) *Channelrhodopsin-2, a directly light-gated cation-selective membrane channel*. Proc Natl Acad Sci, U. S. A. .
69. Foster Kw Fau - Saranak, J., et al. (1984 Oct 2) *A rhodopsin is the functional photoreceptor for phototaxis in the unicellular eukaryote Chlamydomonas*. Nature, 5-31.

70. Boyden Es Fau - Zhang, F., et al. (2005 Sep) *Millisecond-timescale, genetically targeted optical control of neural activity*. Nat, Neurosci.
71. Arenkiel Br Fau - Peca, J., et al. (,2007 Apr 19) *In vivo light-induced activation of neural circuitry in transgenic mice expressing channelrhodopsin-2*. Neuron.
72. Wang H Fau - Peca, J., et al. (Proc Natl Acad Sci, U. S. A.2007 May 8) *High-speed mapping of synaptic connectivity using photostimulation in Channelrhodopsin-2 transgenic mice*. Proc Natl Acad Sci, U. S. A.x.
73. Katzel D Fau - Zemelman, B.V., et al. (2011 Jan) *The columnar and laminar organization of inhibitory connections to neocortical excitatory cells*. Nat, Neurosci.
74. Bruegmann T Fau - Malan, D., et al. (2010 Nov) *Optogenetic control of heart muscle in vitro and in vivo*. Nat, Methods.
75. Bohm M Fau - La Rosee, K., et al., *Evidence for reduction of norepinephrine uptake sites in the failing human heart.* J. Am Coll Cardiol 1995 Jan(0735-1097 (Print)).
76. Zaglia T Fau - Milan, G., et al., *Cardiac sympathetic neurons provide trophic signal to the heart via beta2-adrenoceptor-dependent regulation of proteolysis.* Cardiovasc, Res 2013 Feb 1(1755-3245 (Electronic)).
77. Shcherbakova Og Fau - Hurt, C.M., et al., *Organization of beta-adrenoceptor signaling compartments by sympathetic innervation of cardiac myocytes.* J. Cell Biol 2007 Feb 12(0021-9525 (Print)).
78. Klemm M Fau - Hirst, G.D., G. Hirst Gd Fau - Campbell, and G. Campbell, *Structure of autonomic neuromuscular junctions in the sinus venosus of the toad.* J. Auton Nerv Syst 1992 Jun 15(0165-1838 (Print)).
79. Bennett Mr Fau - Gibson, W.G., J. Gibson Wg Fau - Robinson, and J. Robinson, *Probabilistic secretion of quanta: spontaneous release at active zones of varicosities, boutons, and endplates.* Biophys, J., 1995 Jul(0006-3495 (Print)).
80. Aravanis Am Fau - Wang, L.-P., et al., *An optical neural interface: in vivo control of rodent motor cortex with integrated fiberoptic and optogenetic technology.* J. Neural Eng 2007 Sep(1741-2560 (Print)).
81. Greene La Fau - Tischler, A.S. and A.S. Tischler, *Establishment of a noradrenergic clonal line of rat adrenal pheochromocytoma cells which respond to nerve growth factor.* Proc Natl Acad Sci, U. S. A., 1976 Jul(0027-8424 (Print)).
82. Greene La Fau - Rein, G. and G. Rein, *Synthesis, storage and release of acetylcholine by a noradrenergic pheochromocytoma cell line.* Nature, , 1977 Jul 28(0028-0836 (Print)).
83. Nagel G Fau - Brauner, M., et al., *Light activation of channelrhodopsin-2 in excitable cells of Caenorhabditis elegans triggers rapid behavioral responses.* Curr, Biol 2005 Dec 20(0960-9822 (Print)).
84. Caron Mg Fau - Lefkowitz, R.J. and R.J. Lefkowitz, *Catecholamine receptors: structure, function, and regulation.* Recent Prog Horm, , Res 1993(0079-9963 (Print)).
85. Zipes Dp Fau - Wellens, H.J. and H.J. Wellens, *Sudden cardiac death.* Circulation, x, 1998 Nov 24(0009-7322 (Print)).
86. Rubart M Fau - Zipes, D.P. and D.P. Zipes (2005 Sep) *Mechanisms of sudden cardiac death*. J. Clin Invest

87. Huikuri Hv Fau - Castellanos, A., R.J. Castellanos A Fau - Myerburg, and R.J. Myerburg, *Sudden death due to cardiac arrhythmias.* N. Engl J Med 2001 Nov 15(0028-4793 (Print)).
88. Verkerk Ao Fau - Veldkamp, M.W., et al., *Effects of cell-to-cell uncoupling and catecholamines on Purkinje and ventricular action potentials: implications for phase-1b arrhythmias.* Cardiovasc, Res 2001 Jul(0008-6363 (Print)).
89. Wier Wg Fau - ter Keurs, H.E., et al., *Ca2+ 'sparks' and waves in intact ventricular muscle resolved by confocal imaging.* Circ, Rest, 1997 Oc(0009-7330 (Print)).
90. Baader Ap Fau - Buchler, L., et al. (Res 2002 Jan) *Real time, confocal imaging of Ca(2+) waves in arterially perfused rat hearts*. Cardiovasc, Res.
91. Tanaka H Fau - Oyamada, M., et al., *Excitation-dependent intracellular Ca2+ waves at the border zone of the cryo-injured rat heart revealed by real-time confocal microscopy.* J. Mol Cell Cardiol 2002 Nov(0022-2828 (Print)).
92. Kaneko T Fau - Tanaka, H., et al., *Three distinct types of Ca(2+) waves in Langendorff-perfused rat heart revealed by real-time confocal microscopy.* Circ, Res 2000 May 26(1524-4571 (Electronic)).
93. Wikswo Jp Jr Fau - Lin, S.F., R.A. Lin Sf Fau - Abbas, and R.A. Abbas, *Virtual electrodes in cardiac tissue: a common mechanism for anodal and cathodal stimulation.* Biophys, J. x, Biophys, J. 1995 Dec(0006-3495 (Print)).
94. Campbell Rw Fau - Murray, A., D.G. Murray A Fau - Julian, and D.G. Julian, *Ventricular arrhythmias in first 12 hours of acute myocardial infarction. Natural history study.* Br Heart, J. , 1981 Oct(0007-0769 (Print)).
95. Adgey Aa Fau - Devlin, J.E., et al. (1982 Jan) *Initiation of ventricular fibrillation outside hospital in patients with acute ischaemic heart disease*. 1982 Jan.
96. Johnston Km Fau - MacLeod, B.A., M.J. MacLeod Ba Fau - Walker, and M.J. Walker, *Responses to ligation of a coronary artery in conscious rats and the actions of antiarrhythmics.* Can, J. Physiol Pharmacol 1983 Nov(0008-4212 (Print)).